Electrical Power and Energy Systems 165 (2025) 110472

Contents lists available at ScienceDirect

International Journal of Electrical Power and Energy Systems

journal homepage: www.elsevier.com/locate/ijepes

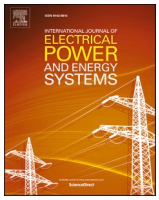

Optimizing smart inverter control for improved distribution network hosting capacity: A model predictive control approach

Muhammad Kamran Khan *, Kimmo Kauhaniemi, Hussain Sarwar Khan

School of Technology and Innovation, University of Vaasa, Finland

ARTICLE INFO

Keywords:
Hosting Capacity
Smart Inverter control
Atomic orbital search optimization (AOS)
Direct power finite control set model predictive control (DP-FCS-MPC)
EN 50549 standard

ABSTRACT

In this work, we investigate Cos Φ and Q(U) control modes of smart inverters as outlined in EN 50549-standards, aiming to improve the hosting capacity (HC) of a real-world distribution network. To improve the HC, an atomic orbital search (AOS) optimization algorithm is employed to determine optimal location and size of DG, along with optimal control setpoints of smart inverters. Furthermore, we delve into the implementation of direct power finite control set model predictive control (DP-FCS-MPC) aimed at augmenting hosting capacity. DP-FCS-MPC operates by directly using active power (*P*) and reactive power (*Q*) as control variables, thus facilitating fast, simple, and decoupled power control without intermediate current loops. The DP-FCS-MPC-based controller regulates the voltage within the targeted limits by tracking the optimal active and reactive power setpoints, directed by the AOS optimizer. The proposed methodology is evaluated using the simulation model of Sundom Smart Grid, a medium voltage distribution network located in Vaasa, Finland. The results confirm the efficacy of the proposed Cos Φ and Q(U) control in improving the HC of the distribution network.

1. Introduction

The Paris Agreement 2015 sketches the greenhouse framework to reduce emission by limiting the global temperature rise under 2°C, with periodic emission mitigation plans [1]. To avert the effects of global warming, the goal of carbon neutrality must be achieved by 2055. In this respect, the European Union (EU) has set a goal to achieve net-zero carbon emission by 2050. To deliver on the European Union's ambitious climate mitigation plans, Finland targeted a 50 % share of energy from renewable generation in gross final power consumption by 2030 [2].

However, the growing integration of renewable energy resources also poses various challenges related to hosting capacity (HC). HC refers to the maximum amount of additional distributed generation (DG) that can be connected to the grid without comprising reliability and stability [3]. Hosting capacity can be limited by various factors, including line and transformer ampacity limits, voltage levels, power quality constraints, and protection coordination [4,5]. The report of Clean Energy Group highlights a notable interconnection issue in Massachusetts, USA, indicating that 2,321 megawatts (MW) of solar capacity and 429 MW of energy storage capacity are in interconnection queues due to the limited hosting capacity of the distribution network [6]. Considering the current scenarios in Finland, according to Yle news if large-scale solar power farms continue to be built in eastern Finland, the capacity of FINGRID transmission network could emerge as a bottleneck.

One of the major constraints that limit the HC of a distribution network is voltage rise particularly during periods of high generation. Therefore, optimal voltage regulation can play a key role in enhancing HC of the distribution network. Most of the modern grid codes i.e. EN 50549–2 [7], IEEE 1547–2018 [8], FINGRID VJV 2018 [9], and California Rule 21–2018 [10] stipulates that generating units wishing to connect to the distribution grid must have the capability to manage reactive and/or active power to keep the voltage within the continuous operating range. DGs are usually connected to the distribution network through power electronic inverters. These smart inverters can operate in all four quadrants and can provide fast and flexible active and reactive support by using various smart inverter (SI) control modes, such as volt-var (Q(U)) and power factor (Cos Φ) control, which can regulate the voltage at the point of connection (PoC i.e. point where DG is connected to the grid). Therefore, SIs equipped with advanced control functions can be a promising option to increase the HC of the distribution network.

Various methods have been proposed in the literature to analyze and improve the hosting capacity of the distribution network [11–13]. In [14], Volt-Var and Volt-Watt control functions were utilized for HC

* Corresponding author.
E-mail address: kamran.khan@uwasa.fi (M.K. Khan).

https://doi.org/10.1016/j.ijepes.2025.110472
Received 4 July 2024; Received in revised form 12 December 2024; Accepted 8 January 2025
Available online 13 January 2025

Table 1
Comparison of control schemes for power converters.

Metric	Linear Control	Sliding mode control	RL-Based Control	MPC
Handling Nonlinearity	No	yes	yes	yes
Predictive Capability	No	No	Implicit (through learning)	yes
Theoretical background	Mature	Mature	Weak	Mature
Robustness	Low	Moderate	High	Moderate
Computational cost	Low	Low	High	High
Constraint Handling	No	Moderate	Implicit (Limited)	Excellent
Ease of Implementation	High	Moderate	low	Moderate to High

maximization and voltage regulation in a distribution network. Also, a new Volt-Var-Watt control mode was proposed to optimally manage active and reactive powers for HC maximization. The research in [15] employed modified particle swarm optimization algorithms to determine optimal power factors that prevent voltage violations across multiple generation, load, and PV allocation scenarios, thus maximizing PV hosting capacity. Furthermore, the research in [16] utilized Monte Carlo simulations to perform HC analysis across seventeen utility distribution feeders. Also, a distribution network management system was proposed that entails optimal operation of capacitors, controllable switches, and smart inverters to maximize HC.

The allocation of DG units, which involves determining the optimal locations and installed capacities, plays a pivotal role in maximizing HC [17,18]. The research in [19] employed two optimization algorithms namely, particle swarm optimization and genetic algorithm, to determine optimal size, location, and inverter control set-points on a real-world distribution feeder. The objective was to maximize PV hosting capacity. The authors claimed a 32.1 % increase in HC with Volt-Var control function. In [20], an equilibrium optimizer-based approach was explored to maximize HC by optimizing locations, sizes, and control settings of Volt-Var functions for multiple PV units. The proposed method was tested on IEEE 123-bus benchmark system through MATLAB and OpenDSS co-simulation. In reference [21], genetic algorithm and particle swarm optimization were proposed to optimize the location, size, and power factor of DG, considering minimization of energy losses and voltage deviations as major objective. In [22], an optimization-based method was proposed to determine HC in distribution networks. The proposed method leverages linear power flow equations for linear programming formulation, enabling near-optimal solutions in a short timeframe. Additionally, in reference [23] slime mould algorithm was used to optimize oversize, dispatch, and control settings of Volt-Var functions for both PVs and BESSs while determining their optimal locations. The goal was to maximize PVHC and minimize voltage deviations simultaneously.

Furthermore, an efficient control technique is required to inject controlled active and reactive powers into the grid. One such control technique is finite control set model predictive control (FCS-MPC), a methodology that can optimally regulate SI inverter switching states to track desired power setpoints [24–26]. Model predictive control (MPC) has attracted increasing attention due to the advantages of the clear concept, high dynamic performance and easy implementation[27]. Furthermore, the classical MPC schemes that require model knowledge can be enhanced via data using learning-based [28,29] and adaptive [30] approaches. In [31], the finite control set learning predictive

Table 2
Comparitive review of studies related to hosting capacity.

Ref.	Objective	DG allocation	Control of SI			Test Network	Solver	Control	Grid code compliance
			Q (U)	Cos Φ	optimization				
[19]	HC maximization	✓		✓	✓	Real Feeder	PSO & GA	–	IEEE 1547
[14]	HC maximization VDM	✓	✓	–	–	Real Feeder	–	PI	IEEE 1547
[22]	HC maximization	–	–	–	–	IEEE 33-bus test system	LP	–	–
[11]	HC estimation	–	–	–	–	IEEE 33-bus test system	MILP	–	–
[12]	HC maximization Loss minimization	–	–	–	–	IEEE 33-bus test system	RPSO	–	–
[18]	HC maximization	✓	✓	–	✓	IEEE 14 & 33-bus system	PSO	–	–
[23]	HC maximization VDM	✓	✓	–	✓	IEEE 33-bus test system	SMA	–	IEEE 1547
[13]	HC maximization	–	✓	–	–	10 bus radial system	–	–	–
[20]	HC maximization	–	–	✓	–	IEEE 123-bus test system	GA	–	–
[42]	HC maximization VDM	–	✓	–	–	–	–	ANN	–
[43]	HC maximization	–	✓	–	–	IEEE 9-bus system	–	MPC	–
[44]	HC maximization	–	✓	–	–	Real Feeder	–	–	–
[17]	HC maximization VDM	✓	–	–	–	IEEE 123 & 137-bus system	COA	–	–
[21]	VDM Power loss minimization	✓	–	✓	✓	IEEE 33-bus test system	PSO & GA	–	–
[20]	HC maximization	✓	✓	–	–	IEEE 123-bus test system	EO	–	–
[45]	VDM Loss minimization	–	✓	–	✓	IEEE 33-bus test system	Cone programming	–	IEEE 1547
[15]	HC maximization	✓	–	✓	✓	Real Feeder	PSO	–	–
This Study	HC maximization VDM	✓	✓	✓	✓	Real Grid	AOS	DP-FCS-MPC	EN 50549

*VDM: Voltage deviation minimization, *PSO: Particle swarm optimization, *GA: Genetic algorithm, *MILP: Mixed-integer linear programming, *SMA: Slime mould algorithm, *EO: Equilibrium optimizer, *COA: Coyote Optimization Algorithm, *ANN: Artificial neural network, *AOS: Atomic orbital search algorithm, *DP-FCS-MPC: Direct power finite control set model predictive control.

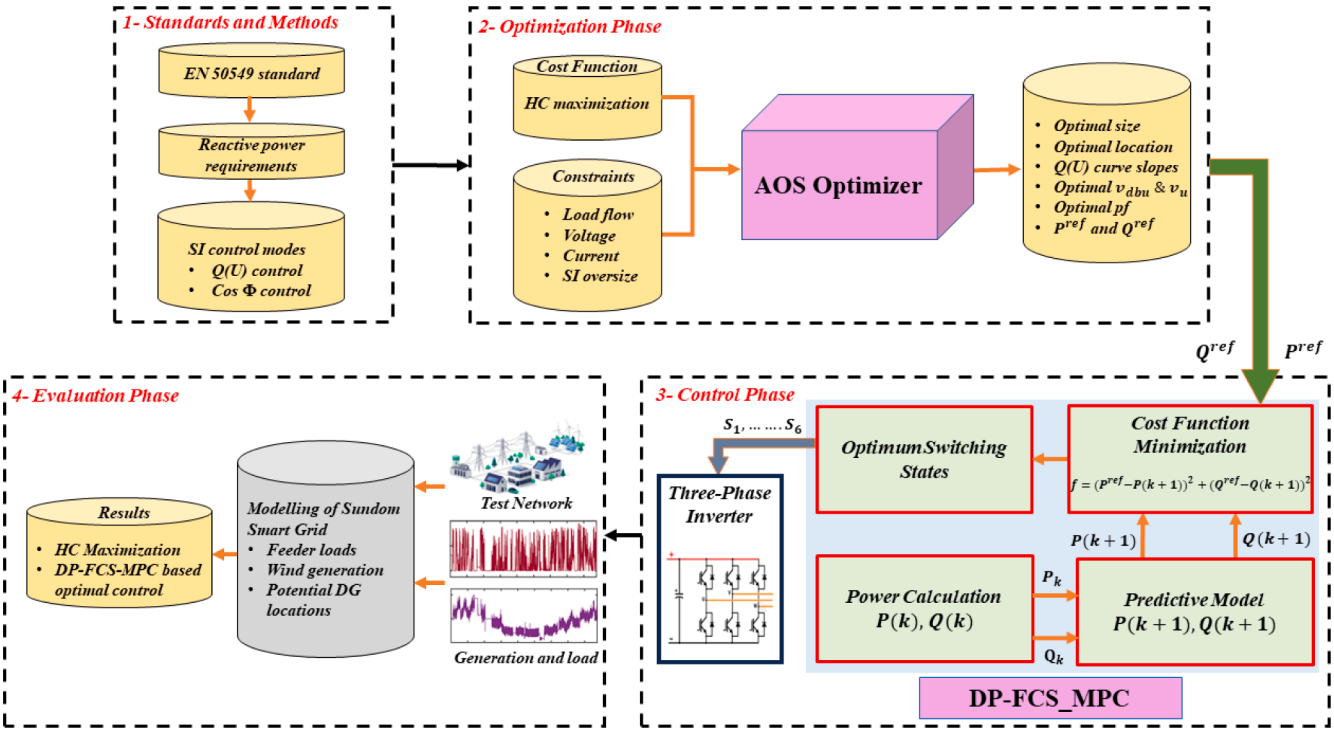

Fig. 1. Graphical Summary of the Research.

control methodology was proposed for power converters to handle unknown dynamics and disturbances. The study in [32] merges the strengths of reinforcement learning with FCS-MPC, offering improved control capabilities when dealing with parametric uncertainties and disturbances.

A comparative analysis of MPC with other control techniques is presented in Table 1.MPC's predictive nature, constraint management, and flexibility make it an advanced and practical choice for modern inverter control, especially in applications requiring high precision and adaptability, such as renewable energy integration and grid support. Within the scope of MPC two main categories emerge: voltage-oriented control (VOC) [33,34] and direct power control (DPC) [35,36]. In general, VOC relies on inner current loops to compute the voltage reference vector and uses space vector pulse width modulation (SVPWM) to generate switching signals for the inverter. In contrast, DPC operates by directly using P and Q as control variables, thus facilitating fast, simple, and decoupled power control without intermediate current loops [37]. Successful implementation of MPC based smart inverter volt-var control has been reported in few research articles [38–41].

1.1. Contributions

A comparative analysis of literature review is presented in Table 2. From the literature review, it is evident that the majority of the prior research has relied on predefined default smart inverter control setpoints, rather than treating them as design variables to optimize. Moreover, there exists a notable gap in research that focuses on investigating modern control techniques specifically aimed at improving hosting capacity. In the light of this context, this research aims to address these research gaps by pursuing two major objectives.

1) The first objective is to maximize the DGHC of the distribution network. In this study, DG refers to both solar PV systems and wind turbines. These technologies share common challenges, such as intermittent generation and their impact on voltage stability. To achieve this objective a nonlinear, non-convex constraint optimization problem is formulated. The atomic orbital search (AOS) algorithm is then employed to determine the optimal location and size for DG installation on a distribution feeder, alongside identifying the most effective control settings for the inverter. Subsequently, utilizing these inverter control setpoints, the optimal reference active and reactive powers (P^{ref}, Q^{ref}) are determined. These reference active and reactive powers are then sent to the controller to facilitate optimal control operation.
2) Secondly, the research aims to explore an efficient control scheme for three-phase grid-tied inverters, that ensures satisfactory steady-state performance and quick transient response. To achieve this, the direct power finite control set model predictive control (DP-FCS-MPC) is utilized. DP-FCS-MPC operates by directly using the active power (P) and reactive power (Q) as control variables, thus facilitating fast, simple, and decoupled power control without intermediate current loops.

This research contributes by addressing both optimization and control aspects, aiming to enhance the performance and hosting capacity of the distribution network, ultimately leading to more efficient and resilient distribution systems. The main contributions of our work are listed below.

- Detailed hosting capacity analysis of the Sundom Smart Grid, a real-world grid located in Vaasa, Finland.
- Investigating the Q(U) and Cos Φ control modes of smart inverters to maximize hosting capacity (HC), while ensuring compliance with EN 50549 standards. The results confirm the efficacy of the proposed Cos Φ and Q(U) control in improving the HC of the distribution network.
- Implementation of Atomic orbital search algorithm (AOS) to optimally determine the location, size, Volt-Var control slopes, and deadband ranges for maximizing hosting capacity. The AOS algorithm exhibits enhanced global convergence and stability, significantly reducing time complexity, ensuring efficient and accurate solutions.
- Implementation of direct power finite control set model predictive control (DP-FCS-MPC) that provide fast, efficient, and decoupled

Table 3
Generator categories based on capacity and operating voltage.

Limits	Generator Types			
	Type A	Type B	Type C	Type D
Operating Voltage	Below 110 kV	Below 110 kV	Below 110 kV	At least 110 kV
Europe	0.8 kW ≤ P_{max} < 1 MW	1 MW ≤ P_{max} < 50 MW	50 MW ≤ P_{max} < 75 MW	P_{max} ≥ 75 MW
Finland	0.8 kW ≤ P_{max} < 1 MW	1 MW ≤ P_{max} < 10 MW	10 MW ≤P_{max} < 30 MW	P_{max} ≥ 30 MW
Great Britain	0.8 kW ≤ P_{max} < 1 MW	1 MW ≤P_{max} < 10 MW	10 MW ≤P_{max} < 30 MW	P_{max} ≥ 30 MW
Ireland	0.8 kW ≤ P_{max} < 0.1 MW	0.1 MW ≤ P_{max} < 5 MW	5 MW ≤P_{max} < 10 MW	P_{max} ≥ 10 MW
Baltic	0.8 kW ≤ P_{max} < 0.5 MW	0.5 MW ≤ P_{max} < 10 MW	10 MW ≤P_{max} < 15 MW	P_{max} ≥ 15 MW

control. The controller exhibits excellent transient and steady-state response, meeting the tracking requirements specified in the EN 50549 standards.

- Proposing a novel optimal control framework in which DP-FCS-MPC-based controller regulates the voltage within the targeted limit by tracking the reference active and reactive power setpoints, directed by the AOS optimizer. The proposed control framework proactively manages voltage levels, maximizes hosting capacity, and ensure grid stability under varying DG generation scenarios.

The main steps of this research are graphically illustrated in Fig. 1. These steps include an overview of EN 50549 standard (Section 2), modelling of smart inverter control modes (Subsection 3.1), HC enhancement as optimization problem (Subsection 3.2), proposed optimal control methodology (Section 4), test network and simulation results (Section 5).

2. Overview of grid codes

Grid codes provide a collection of technical specifications and rules that guide how electrical networks operate and interact. These collaboratively developed standards aid interoperability and coordination between various components of the power system. The grid codes ensure reliable, secure, and economic functioning of the electric grid. Different countries may have different grid code requirements based on their infrastructure, energy sources, and regulatory frameworks. Grid code compliance gives confidence to the distribution system operator that asset wishing to connect to the grid will not endanger the security of the supply.

2.1. EN 50549 standard

EN 50549–1 and EN 50549–2 are grid-integration standards that are issued by CENELEC in 2019. EN 50549–1 and EN 50549–2 specify requirements for type A and type B generating plants connected to and operated in parallel with low voltage and medium voltage distribution network respectively. Generators can be classified into four categories based on generating capacity and operating voltage as explained in Table 3. Most European countries follow EN 50549 standard as a reference for the grid connection of distributed energy resources (DERs). The architecture and evolution of EN 50549 series is shown in Fig. 2.

2.2. Voltage support by reactive power

From a European perspective, grid codes increasingly require inverter based distributed generation to provide various ancillary services to the grid. According to EN 50549 standard the DG shall have the capability of managing reactive and/or active power generation, when voltage support is required by distribution system operators (DSOs). The Generating units wishing to connect to the distribution grid must have the capability to manage reactive and/or active power to keep the voltage within the continuous operating range. The continuous operating voltage range, as defined in EN 50549 standard, lies between 90 to 110 % of the nominal operating voltage at PoC.

Furthermore, EN 50549 standard stipulates that the DSO and the responsible party (transmission system operator or regulating authority) shall decide the reactive power requirements. However, if no such requirements are defined then the default reactive power requirements are:

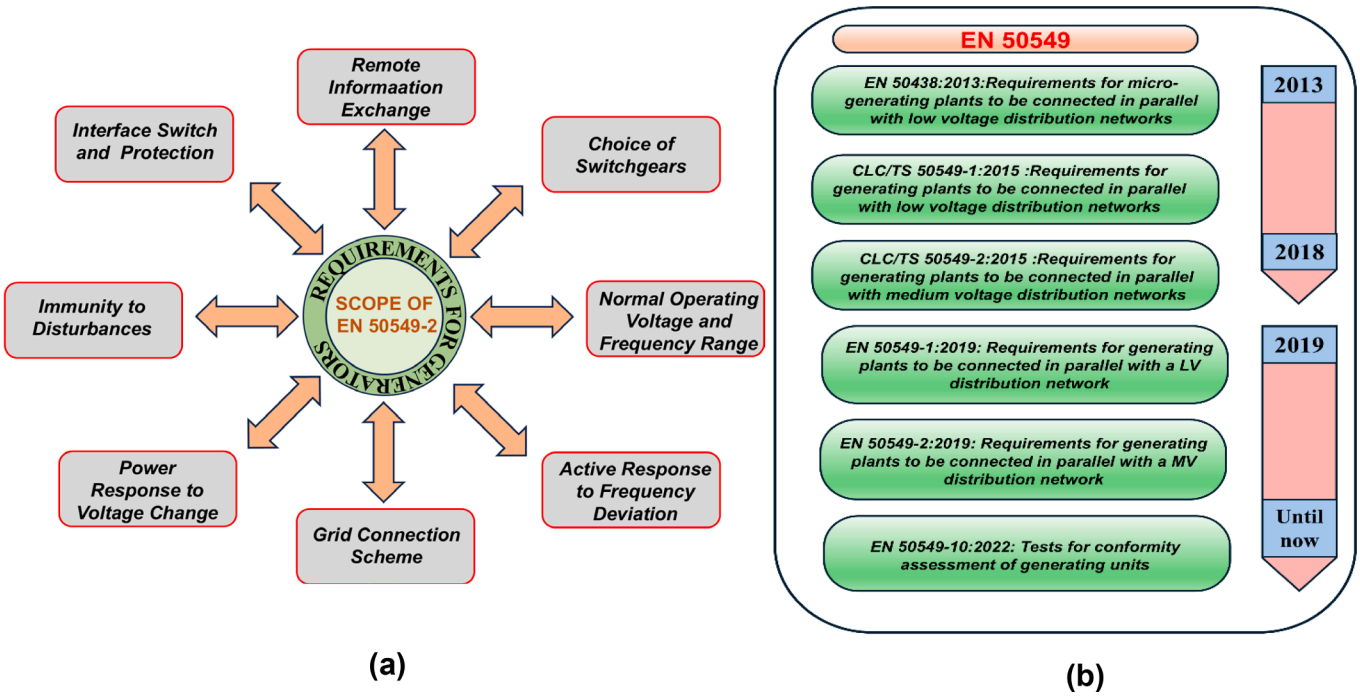

Fig. 2. (a) Scope of EN-50549 (b) Evolution of EN-50549.

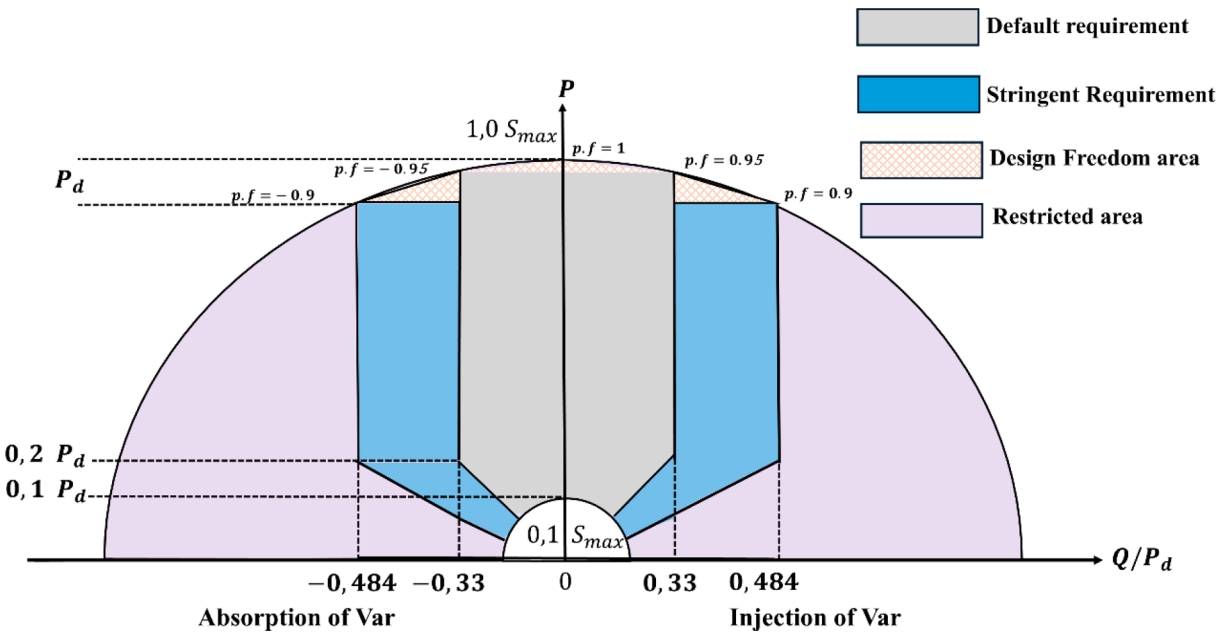

Fig. 3. Required Reactive Power Capability according to EN 50549–2.

Table 4
Smart inverter control modes in different standards.

Control Modes	STANDARDS			
	EN 50,549	IEEE 1547	FINGRID VJV 2018	California Rule-21
Q setpoint	✓*	✓	✓*	
Q(V)	✓	✓	✓	✓*
Q(P)	✓	✓		✓
Cos Φ setpoint	✓	✓*	✓	✓
Cos Φ(P)	✓			
P(V)	✓	✓		

*: Default control mode.

- When active power (P) is greater than 20 percent of the demanded power P_d, generating unit shall have the capability to inject/absorb reactive power (Q) up to 33 % of the P_d.
- If P is less than 20 percent of P_d, the generating unit should have the capability to inject/absorb Q according to Fig. 3.
- Considering stringent requirements, generating units should have the capability to inject/absorb reactive power up to 48.4 % of the P_d, when P is greater than 20 % of P_d.
- Similarly, if P is less than 20 percent of P_d, the stringent Q requirements should be according to Fig. 3.

Fig. 3 gives a graphical representation of the minimum and optional capabilities at nominal voltage. The default requirements are less demanding and are meant to ensure a basic level of compatibility with the grid. According to EN 50549–2, the default reactive power requirements (depicted by the grey region of figure) are 33 % of the demanded active power P_d, which corresponds to a power factor of 0.95. When operating at active power below 20 % P_d reactive power shall be provided according to Fig. 3 to a minimum power factor of 0.52. The stringent requirements (depicted by blue region in figure) are more demanding and aim to enhance grid support. According to stringent requirements, inverters must operate within a wider power factor range, 0.9 leading to 0.9 lagging, which corresponds to the reactive power injection/absorption capability of up to 48.4 % of the P_d. When operating at active power below 20 % P_d reactive power shall be provided according to Fig. 3 to a minimum power factor of 0.38. Furthermore, generating units manufactures have flexibility in sizing the output capacity to balance operational benefits and drawbacks. For example, oversizing can help minimize active power curtailment when meeting EN 50549 requirements, such as managing voltage fluctuations or reactive power exchange. This is indicated by the design freedom area in Fig. 3.

In case of overvoltage, EN 50549–2 permits the exchange of additional reactive power up to the rated current, thereby allowing an increase in the apparent power. Moreover, generating units shall have the capability of operating in the control modes outlined in Table 4. The Cos Φ setpoint and Q setpoint modes control the power factor and reactive power respectively, according to the predetermined setpoints. The Q(U) mode regulates reactive power output as a function of voltage. The Q(P) and Cos Φ(P) control the reactive power and the power factor respectively based on the changes in the active power output.

3. Modelling and problem formulation

EN 50,549 stipulates that generating plants shall have a capability to inject/absorb reactive power in the range of 0 to 48.4 % of demanded active power (P_d). Furthermore, from Fig. 3 it can be seen that the required reactive power range corresponds to the power factor variations from ± 0.9 to 1. However, no guidelines are provided regarding optimal reactive power that should be injected when voltage exceeds the continuous operating range. Under various load and generation conditions, it is possible to restore the voltage within the continuous operating region by injecting/absorbing Q less than the specified upper limits (48.4 %). In such scenarios, unnecessary injection/absorption of Q can potentially overload the distribution network, creating a hosting capacity bottleneck. This hosting capacity bottleneck can be alleviated by determining optimal slopes in case of Q(U) control or by choosing optimal power factors in Cos Φ control, thus maximizing renewable energy penetration, and increasing the hosting capacity.

3.1. Modelling smart inverter control functions

DGs are usually connected to the distribution network through power electronic inverters. These inverters can operate in all four quadrants and in addition to supplying active power they can also inject or absorb reactive power. From a European perspective, grid codes

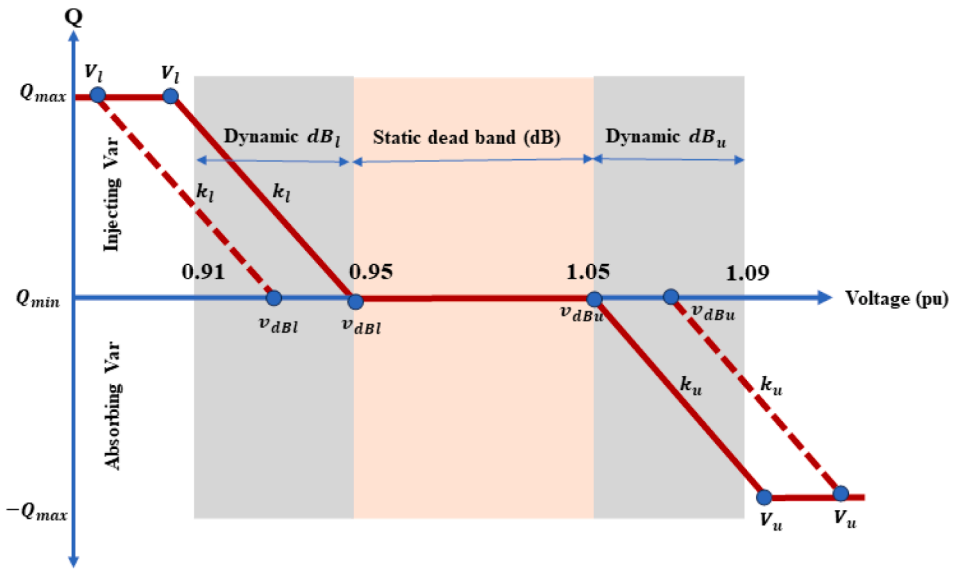

Fig. 4. Q(U) curve.

increasingly require distributed generators to provide both static and dynamic voltage support. In this research, the Cos Φ and Q(U) control modes are selected for their widespread adaptation and their proven effectiveness in voltage regulation.

3.1.1. Cos Φ control

In Cos Φ control, smart inverter regulates both active and reactive power based on the selected power factor (*pf*). The *pf* can be adjusted within the range of ± 0.9 to 1. When operating at unity power factor, smart inverter exports all the generated active power to the grid. A *pf* of 0.9 implies 11.12 % curtailment in the available active power to create head room for reactive power as oversizing of inverter is not considered in the proposed Cos Φ Control. When SI is operating in Cos Φ mode, the reactive power output is dynamically adjusted based on the voltage magnitudes and the specified power factor settings, as modelled in (1).

$$\begin{cases} P_{DG} = S_{DG} \\ Q_{DG} = 0 \end{cases}, if v^{min} < v_{poc} < v^{max}$$
$$\begin{cases} P_{DG} = S_{DG} * pf \\ Q_{DG} = \alpha(P_{DG} * tan(cos^{-1}(pf))) \end{cases}, if v^{min} > v_{poc} > v^{max} \quad (1)$$

$$\alpha = \frac{v_{ref} - v_{poc}}{|v_{ref} - v_{poc}|} \quad (2)$$

Here P_{DG}, Q_{DG}, and S_{DG} are the active, reactive, and apparent powers from the DG. α represents the sign index. The value of α could be either 1 or −1. The positive value of α means *pf* is leading, and reactive power should be injected while negative value of α implies reactive power absorption. v_{poc} is measured voltage at the point of connection, v^{min} & v^{max} are the specified lower and upper voltage limits and $v_{ref} = 1$. Equation (1) clearly shows that, as the *pf* decreases, the curtailment of active power increases to accommodate the necessary reactive power. By selecting optimal power factor settings, the smart inverter can effectively manage reactive power outputs, ensuring minimum curtailment and maximum HC.

3.1.2. Q(U) control

In the proposed Q(U) control, the smart inverter employs a combination of fixed and dynamic dead bands, along with optimal slopes, to effectively regulate reactive power output in response to the variations in grid voltage. The Q(U) curve shown in Fig. 4, illustrates how reactive power of the inverter varies with changes in voltage magnitudes. In the proposed scheme static and dynamic dead bands are introduced to accommodate various voltage ranges. Within the static dead band range, set between 0.95 pu to 1.05 pu, inverter does not provide any reactive power support. This means that when the voltage at PoC falls within this range, the inverter remains inactive in terms of *Q* support. However, when the voltage at PoC falls within the dynamic dead bands the inverter can respond to the voltage variations by managing reactive power.

The upper and lower dynamic dead bands are not fixed. The upper dynamic dead band can vary between 1.05 V (pu) to 1.09 V (pu), while the lower dynamic dead band can vary between 0.95 V (pu) to 0.91 V (pu), respectively. In this study, dynamic dead bands are optimized to maximize HC by selecting optimal v_{dbu} and v_{dbl}. When the voltage at PoC is greater than v_{dbu}, the inverter operates in inductive mode and absorbs reactive power. Conversely, if v_{poc} is less than v_{dbl}, the inverter operates in capacitive mode and injects reactive power. Additionally, when v_{poc} is between v_{dbu} and v_u or between v_{dbl} and v_l, the smart inverter absorbs or injects reactive power based on predefined slopes k_u and k_l respectively. These slopes determine the rate at which the inverter absorbs or injects reactive power. Therefore, by selecting optimal volt-var setpoints, smart inverters can effectively regulate reactive power to maximize HC. The reactive power as a function of voltage and control setpoints can be expressed mathematically as:

$$Q_{DG} = S_{DG} * \begin{cases} \alpha(|v_{poc} - v_{dBu}|)\, k_u, if v_{poc} > v_{dBu} \\ \alpha(|v_{poc} - v_{dBl}|)k_l, if v_{poc} < v_{dBl} \\ \alpha * 0.484, if v_u > v_{poc} > v_l \\ 0, if v_{dBl} < v_{poc} < v_{dBu} \end{cases} \quad (3)$$

$$k_{u,l} = \frac{Q_{max} - Q_{min}}{v_{u,l} - v_{dbu,dbl}} \quad (4)$$

Furthermore, it is worth noting that in Q(U) control inverter is oversized to create head room for reactive power. For reactive power injection/absorption of 48.4 % of the P_d, the inverter is oversized by 11.12 %. Therefore,

$$P_{DG} = S_{DG} \quad (5)$$

3.2. Problem formulation

The hosting capacity maximization problem is formulated as a non-linear, non-convex constraint optimization problem. The objective function is to maximize the DGHC of the distribution network.

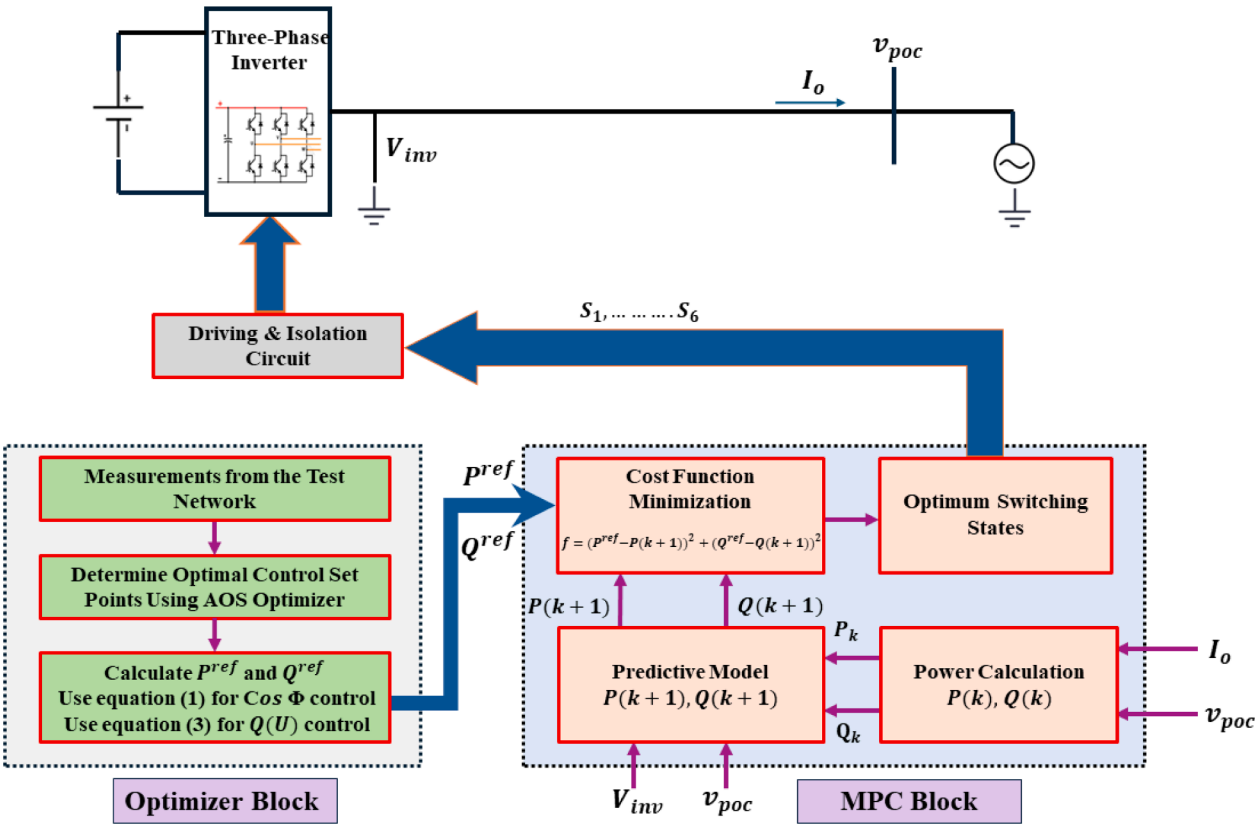

Fig. 5. Proposed optimal control methodology.

$$\underset{x}{Max} \sum_{d=1}^{N_{DG}} P_{DG,d}^{Gen} \tag{6}$$

Here, the vector $x = [n, S_{DG}, pf, k_l, k_u, v_{dBu}, v_{dBl}]^T$, represents set of decision variables which includes location, size and setpoints of the smart inverter control. N_{DG} represents the number of buses that contain DGs. The set of potential DG locations is represented by n and S_{DG} represents size of the DG. In case of Cos Φ control the control setpoint is power factor (pf); while control setpoints for Q(U) control are $k_l, k_u, v_{dBu}, and v_{dBl}$.

The HC maximization problem is subject to the following constraints:

$$P^g + P_j^{DG} - P_j^D = |V_j| \sum_{k=1}^{N_{bus}} |V_k| \left(G_{jk} cos\theta_{jk} + B_{jk} sin\theta_{jk}\right) \tag{7}$$

$$Q^g + Q_j^{DG} - Q_j^D = |V_j| \sum_{k=1}^{N_{bus}} |V_k| \left(G_{jk} sin\theta_{jk} + B_{jk} cos\theta_{jk}\right) \tag{8}$$

Here, P^g and Q^g represent active and reactive powers from the grid respectively; P_j^{DG} and Q_j^{DG} are the active and reactive powers of distributed generators; P_j^D and Q_j^D are the active and reactive load demands; N_{bus} represent total number of buses in the distribution network; V_j and V_k are the voltages of buses j and k; G_{jk} and B_{jk} are the real and imaginary part of Y_{bus} matrix corresponding to j-th row and k-th column; θ_{jk} is the voltage angle difference between bus j and k. Equations (9), (10) & (11) represent voltage, current and DG installed capacity limits.

$$V^{min} \leq V_j \leq V^{max} \forall j \in N_{bus} \tag{9}$$

$$I_{jk} \leq I_{jk}^{rated} \forall j \in N_{bus} \tag{10}$$

$$S_{DG}{}^{min} \leq S_{DG,j} \leq S_{DG}{}^{max} \forall j \in N_{DG} \tag{11}$$

Moreover, inverter oversized limits and power factor (pf) limits of Cos Φ control are represented by Equations (12) and (13), respectively. Also, the slope ($k_j^{u,l}$) limits, variable dead band upper and lower limits ($v_{dBj}^{u,l}$) and upper and lower voltage ($v_j^{u,l}$) limits that defines Q(U) curve of the smart inverter at bus j are given by equations (14), (15), and (16), respectively.

$$S_{DG,os}{}^{min} \leq S_{DG,os} \leq S_{DG,os}{}^{max} \tag{12}$$

$$pf^{min} \leq pf_j \leq pf^{max} \forall j \in N_{DG} \tag{13}$$

$$k^{min} \leq k_j^{u,l} \leq k^{max} \forall j \in N_{DG} \tag{14}$$

$$v_{dB}{}^{min} \leq v_{dBj}^{u,l} \leq v_{dB}{}^{max} \forall j \in N_{DG} \tag{15}$$

$$v_{u,l}{}^{min} \leq v_j^{u,l} \leq v_{u,l}{}^{max} \forall j \in N_{DG} \tag{16}$$

4. Methodology

The methodology of the proposed DP-FCS-MPC based optimal control for a three-phase grid-connected inverter is illustrated in Fig. 5. The system is composed of two main blocks: (1) the Optimizer block, which determines the optimal reference active and reactive power signals (P^{ref} & Q^{ref}) using atomic orbital search algorithm such that DGHC can be maximized; (2) the MPC block, which select inverter switching states such that active and reactive powers injected to the grid from the DG are directly controlled to their reference values (P^{ref} & Q^{ref}).

4.1. Atomic orbital search (AOS) optimization

The atomic orbital search (AOS) optimizer is used to determine optimal active and reactive power reference points by solving the optimization problem formulated in section 3.2. The AOS is selected because

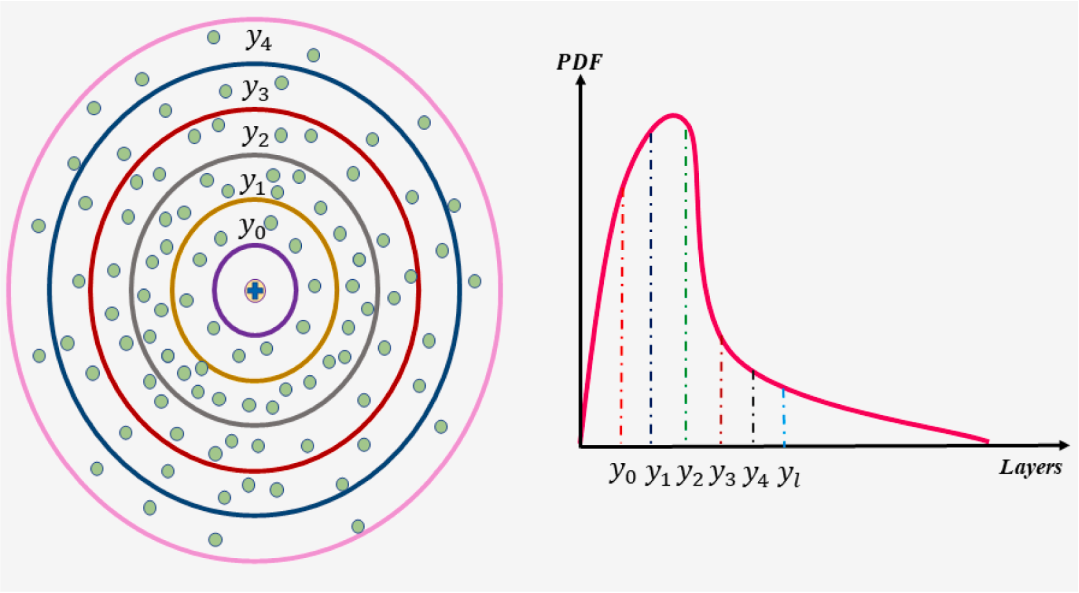

Fig. 6. Distribution of potential candidates using PDF.

it is simple, requires only a single tuning parameter, uses dynamic weights that adjust according to the number of iterations to achieve a perfect balance between exploitation (refining and utilizing known solutions) & exploration (searching for new solutions) and has an excellent global optimum finding capability.

4.1.1. Mathematical modeling

The AOS optimizer uses analogy of electrons around a nucleus to conceptualize the optimization process [46]. In this algorithm imaginary distributed layers around the nucleus represent the search space, while the electrons represent potential solution candidates. The energy level of an electron is analogous to the objective function. The electrons are distributed in imaginary layers around the nucleus using a Probability Density Function (PDF) as shown in Fig. 6. The electrons with lower energy levels represent the better solution candidates, while those with higher energy levels represent solution candidates with the worst fitness value. The algorithm is initialized using equation (17).

$$p_c^m(0) = p_{c,min}^m + rand \times \left(p_{c,max}^m - p_{c,min}^m\right), \begin{cases} c = 1, 2, \cdots.., t \\ m = 1, 2, \cdots., d \end{cases} \tag{17}$$

$p_c^m(0)$ is the initial position of the solution candidates in the m-th dimension. $p_{c,max}^m$ and $p_{c,min}^m$ represent the maximum and minimum limits, and *rand* is the random number between 0 and 1. Here, t represents the total number of solution candidates and d is the dimension of the problem.

The binding state (BS^y) and binding energy (BE^y) in the y-th hypothetical layer can be calculated by averaging the positions and objective function values of solution candidates.

$$BS^y = \frac{\sum_{c=1}^{t} p_c^y}{t}, \quad \begin{cases} c = 1, 2, \cdots., t \\ y = 1, 2, \cdots., l \end{cases} \tag{18}$$

$$BE^y = \frac{\sum_{c=1}^{t} E_c^y}{t}, \begin{cases} c = 1, 2, \cdots., t \\ y = 1, 2, \cdots., l \end{cases} \tag{19}$$

Here, p_c^y represents the location and E_c^y is the fitness value of solution candidate in layer y; y represents number of layers and c shows potential solution candidates in a particular layer. Similarly,

$$BS = \frac{\sum_{c=1}^{t} p_c}{z}, c = 1, 2, \cdots.., t \tag{20}$$

$$BE = \frac{\sum_{c=1}^{t} E_c}{z}, c = 1, 2, \cdots.., t \tag{21}$$

Here, BE and BS refers to the binding energy and binding state in the whole search space respectively; E_c and p_c represents the fitness value and location of the c-th solution candidate, respectively. Photon rate determines the likelihood of the photon action on an electron. A uniformly distributed random number (θ) between 0 and 1 mathematical represents the potential of photon action. If the likelihood of photon action is low, the optimizer further explores the search space by using (22).

$$p_{c+1}^y = p_c^y + u_c \begin{cases} c = 1, 2, 3, \cdots.., t \\ y = 1, 2, 3, \cdots.., l \end{cases} \tag{22}$$

Here, p_c^y and p_{c+1}^y are the current and updated locations for the electrons of layer y; u_c represents random number that lies between 0 and 1. The control parameter photon rate (*pr*) is important in determining the balance between exploitation and exploration phases. Lower value of *pr* results in large exploitation but it may limit the exploration of the search space and vice versa. In a particular layer if $E_c^y \geq BE^y$, the potential candidates are updated using (23).

$$p_{c+1}^y = p_c^y + \frac{\beta_c \times (\gamma_c \times LE - \delta_c \times BS)}{y} \begin{cases} c = 1, 2, 3, \cdots.., t \\ y = 1, 2, 3, \cdots.., l \end{cases} \tag{23}$$

p_c^y and p_{c+1}^y are the current and updated positions for potential candidates; LE = global best position; βc, γ_c and δ_c are the random numbers between 0 and 1. If $E_c^y \leq BE^y$, the position is modified using:

$$p_{c+1}^y = p_c^y + \beta_c \times (\gamma_c \times LE^y - \delta_c \times BS^y) \begin{cases} c = 1, 2, 3, \cdots.., t \\ y = 1, 2, 3, \cdots.., l \end{cases} \tag{24}$$

Here, LE^y represent best position in layer y; βc, γ_c and δ_c are uniform random numbers between 0 and 1.

4.1.2. Proposed AOS based HC enhancement

The objective is to maximize DG active power generation (Fitness Function) by properly choosing decision variables (location of electrons). The decision variable vector x for Q(U) and Cos Φ control is mathematically represented in (25).

$$\begin{cases} x = [n\ S_{DG}\ k_l\ k_u\ v_{dBu}\ v_{dBl}]^T, forQ(U)control \\ x = [n\ S_{DG}\ pf]^T, forCos\Phi control \end{cases} \tag{25}$$

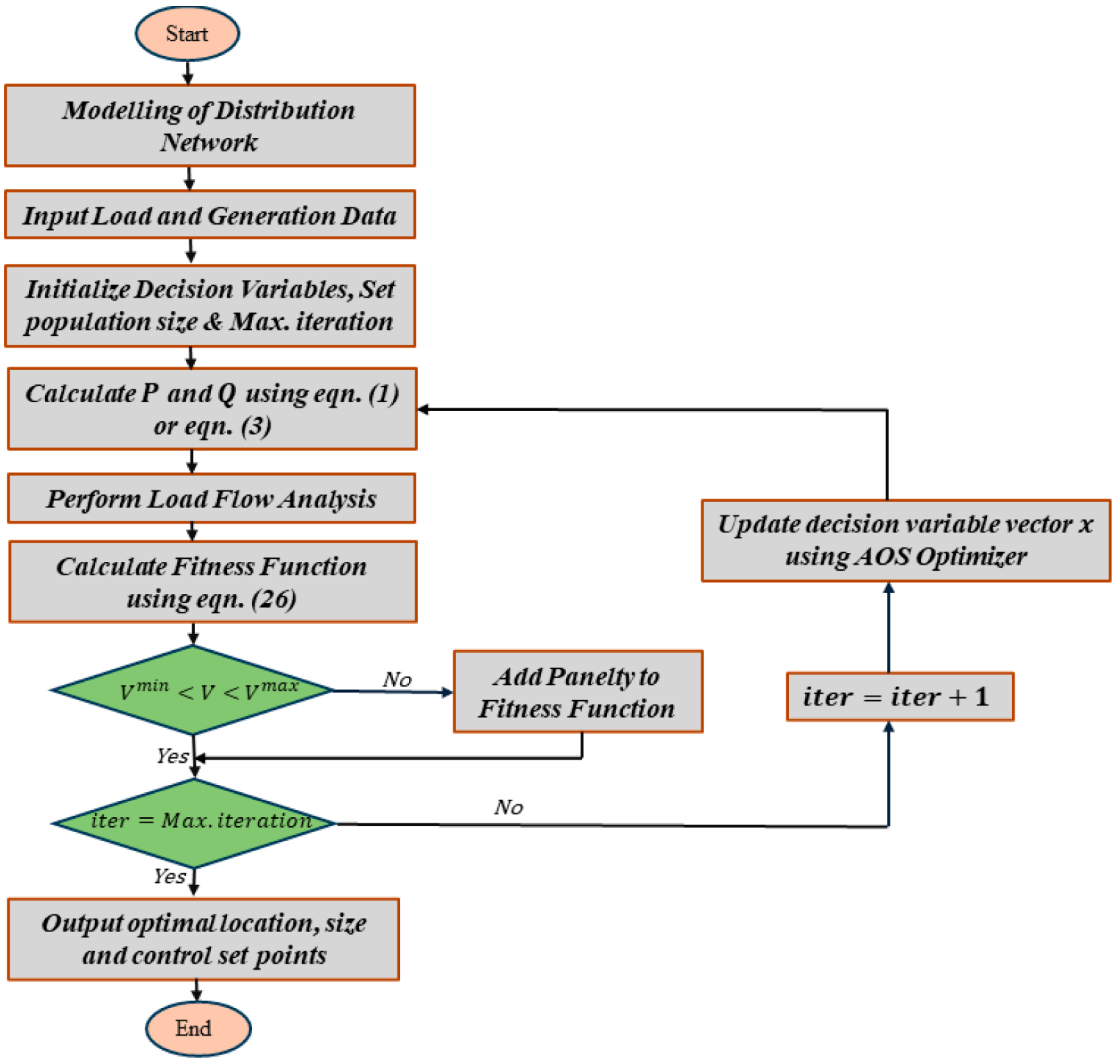

Fig. 7. Flowchart of proposed HC enhancement method.

where n and S_{DG} represent location and size of DG, pf is the power factor, k_l & k_u are the Q(U) curve slopes, and v_{dBu} & v_{dBl} are the upper and lower deadband limits. The fitness function for Q(U) and Cos Φ control is,

$$\begin{cases} P_{DG}^{gen} = S_{DG}, forQ(U)control \\ P_{DG}^{gen} = S_{DG}{*}pf, forCos\Phi control \end{cases} \quad (26)$$

The purpose of utilizing smart inverter control is to optimally manage reactive power in such a way that the active power of DG can be maximized without violating the constraints. The reactive power as a function of decision variable x is calculated by using equation (1) for Cos Φ control and equation (3) for Q(U) control as derived in section 3.1.

A flow chart representation of the proposed method is shown in Fig. 7. First, distribution network is modelled by collecting power system parameters, load data and renewable generation data. Then, AOS optimizer parameters such as size and dimensions of the populations (x), max iteration, iteration counter and photon rate are initialized. Utilizing the initial population active and reactive powers are calculated using equations derived in section 3.1. After that, a load flow analysis is performed to determine bus voltages, currents, active and reactive power flow between buses. Then, fitness function is calculated using equation (26) for the initialized population, and the decision variables that give best fitness function value are sorted. If any of the operational constraints as specified by equations (9) and (10) in section 3.2 is violated, the fitness function is penalized. We add a maximum penalty and make fitness function value zero if any of the operational constraint is violated. Subsequently AOS optimizer is used to determine a new set of candidate solutions for the next iteration and the whole process is repeated until the stopping criteria is met. Finally, when maximum iterations are reached, the best location, size of DG and control setpoints, which gives maximum fitness function (hosting capacity) value are selected as output.

4.2. Direct power model predictive control

Recently, FCS-MPC has emerged as a prominent technique, offering robust and flexible control for grid-tie inverters. FCS-MPC is employed to apply a direct PQ control strategy such that the active and reactive powers (P and Q) injected to the grid from the DER are directly controlled to their reference values.

4.2.1. Control problem formulation

The aim of the DP-FCS-MPC controller is to enable flexible power regulation. Therefore, control objective can be written as:

$$f = (P^{ref} - P(k+1))^2 + (Q^{ref} - Q(k+1))^2 \quad (27)$$

where P^{ref} and Q^{ref} are the desired active and reactive powers to be injected to the grid through the 3-Φ inverter. The first term of the cost function aims to minimize the active power deviation, while the second

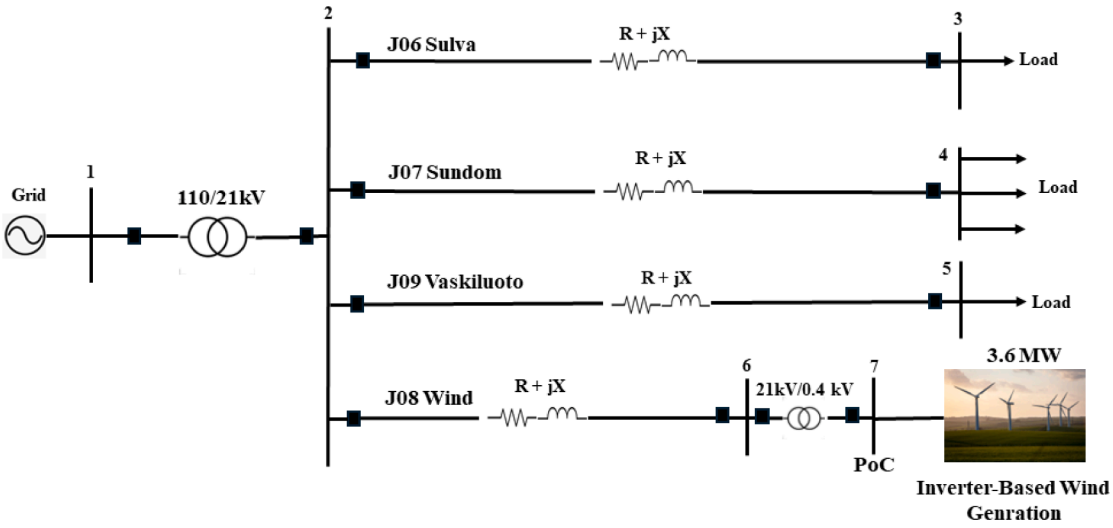

Fig. 8. Sundom smart grid test network.

term aims to minimize the reactive power deviation. Solving a Model Predictive Control (MPC) problem for flexible power regulation typically involves the following three steps: (a) Defining system model, (b) developing prediction models to forecast future states over a predefine prediction horizon, and (c) determining optimal control actions to minimize the selected cost function [37].

a) Defining system model: The MPC controller uses system model to predict system behavior at each sampling instant. For achieving flexible power regulation, an inverter model is designed using active and reactive power as state variables. As depicted in Fig. 5, the mathematical model of the grid-connected inverter system can be described in orthogonal αβ reference frames as:

$$V_{inv} = L\frac{dI_o}{dt} + RI_o + v_{poc} \tag{28}$$

Here, $V_{inv} = \left[V_{inv,\alpha} \;\; V_{inv,\beta}\right]^T$ is the inverter voltage, $v_{poc} = \left[v_{poc,\alpha} \;\; v_{poc,\beta}\right]^T$ is the voltage at the point of connection and, $I_o = \left[I_{o,\alpha} \;\; I_{o,\beta}\right]^T$ is the line current. Specifically, the inverter can be controlled to produce seven distinct voltage vectors that correspond to a specific combination of inverter switching states, as modelled in equation (29).

$$V_{inv,s} = \begin{cases} 0, s = 0, 7 \\ \frac{2}{3}V_{dc}e^{j(s-1)\frac{\pi}{3}}, s = 1, \cdots, 6 \end{cases} \tag{29}$$

Also, considering a balance three-phase system, we can write:

$$\frac{dv_{poc,\alpha}}{dt} = -\omega^* v_{poc,\beta} \tag{30}$$

$$\frac{dv_{poc,\beta}}{dt} = \omega^* v_{poc,\alpha} \tag{31}$$

Where ω is the angular frequency. To implement direct power model predictive control a system model is required that uses active and reactive powers as state variables. The state equations that govern active and reactive power injection by a grid-tie inverter can be mathematically expressed as:

$$x = \begin{bmatrix} P \\ Q \end{bmatrix} = \frac{3}{2}\begin{bmatrix} v_{poc,\alpha} & v_{poc,\beta} \\ v_{poc,\beta} & -v_{poc,\alpha} \end{bmatrix}\begin{bmatrix} I_{o,\alpha} \\ I_{o,\beta} \end{bmatrix} \tag{32}$$

Taking derivate of state variable $x = [P \;\; Q]^T$ yields

$$\begin{bmatrix} \frac{dP}{dt} \\ \frac{dQ}{dt} \end{bmatrix} = \frac{3}{2}\begin{bmatrix} \frac{dv_{poc,\alpha}}{dt} & \frac{v_{poc,\beta}}{dt} \\ \frac{v_{poc,\beta}}{dt} & -\frac{v_{poc,\alpha}}{dt} \end{bmatrix}\begin{bmatrix} I_{o,\alpha} \\ I_{o,\beta} \end{bmatrix} + \frac{3}{2}\begin{bmatrix} v_{poc,\alpha} & v_{poc,\beta} \\ v_{poc,\beta} & -v_{poc,\alpha} \end{bmatrix}\begin{bmatrix} \frac{dI_{o,\alpha}}{dt} \\ \frac{dI_{o,\beta}}{dt} \end{bmatrix} \tag{33}$$

Combination of equations 28–31, 32 and 33 gives state-space equation of the grid connected inverter with P and Q as state variables.

$$\frac{dx}{dt} = \begin{bmatrix} \frac{dP}{dt} \\ \frac{dQ}{dt} \end{bmatrix} = Ax + \frac{3}{2L}BV_{inv} - \frac{3}{2L}Cv_{poc} \tag{34}$$

Here,

$$A = \begin{bmatrix} -\frac{R}{L} & -\omega \\ \omega & -\frac{R}{L} \end{bmatrix} \tag{35}$$

$$B = \begin{bmatrix} v_{poc,\alpha} & v_{poc,\beta} \\ v_{poc,\beta} & -v_{poc,\alpha} \end{bmatrix} \tag{36}$$

$$C = \begin{bmatrix} v_{poc,\alpha} & v_{poc,\beta} \\ 0 & 0 \end{bmatrix} \tag{37}$$

Equation (34) represents grid-tied inverter by a state-space model with inverter voltage (V_{inv}) as the input, and P & Q as the state variables (x); v_{poc} can be measured. The state-space model describes how the active and reactive power states evolve over time based on state variables (P and Q) and inputs (V_{inv} and v_{poc}).

b) Developing prediction model: In the second step a prediction model is developed to forecast future states over a predefined prediction horizon. Considering the sampling time T_s, a prediction model can be formulated.

$$P(k+1) = P(k) + \left[AP(k) + \frac{3}{2L}BV_{inv}(k) - \frac{3}{2L}Cv_{poc}(k)\right]T_s \tag{38}$$

$$Q(k+1) = Q(k) + \left[AQ(k) + \frac{3}{2L}BV_{inv}(k) - \frac{3}{2L}Cv_{poc}(k)\right]T_s \tag{39}$$

Equations (38) & (39) can be used to predict the behavior of state variables (P and Q) in terms of voltage space vectors $V_{inv,s}$ for the next step, as illustrated in MPC block of Fig. 5. The measurements of the line currents (I_o) and grid voltages (V_{inv} & v_{poc}) are used to calculate the

Table 5
Details of the test Network.

Sundom Grid	Details
Number of metering points	2500 (Residential and small commercial users)
Maximum wind generation	3.6 MW
No. of feeders	4
Length of feeders	J06 Sulva: 25.24 km (Overhead line) + 7.93 km (Cable) = 33.18 km J07 Sundom: 12.95 km (Overhead line) + 10.19 km (Cable) = 23.14 km J08 Wind: 0 km (Overhead line) + 0.733 km (Cable) = 0.733 km J09 Vaskiluoto: 5.91 km (Overhead line) + 1.12 km (Cable) = 7.03 km
Conductors Used	AHXCMK-W 3x185, Sparrow AF40, Raven AF62, Swan AF25, AHXW 185, AHXW 3x95, AL 132, SAX-W 50

active power $P(k)$ and reactive power $Q(k)$ at the current sampling instant k. Equations (38) & (39) are then employed to predict the power values at the next sampling instant $P(k+1)$ and $Q(k+1)$, for all possible voltage space vectors (7 in this case).

c) Cost function minimization: The optimal space vector for the next sampling period is determined by comparing predicted power with reference power using a cost function as defined in equation (40). Each voltage vector is evaluated utilizing the cost function. The voltage vector that minimizes the differences is chosen and applied at the next sampling period. The utilized cost function is:

$$f = (P^{ref} - P(k+1))^2 + (Q^{ref} - Q(k+1))^2 \quad (40)$$

Here, P^{ref} and Q^{ref} represent the desired values of the active and reactive powers optimally determined by the AOS optimizer, while $P(k+1)$ and $Q(k+1)$, are the predicted active and reactive powers. To minimize this cost function, the control algorithm adjusts inverter output to match the predicted power with the desired power, thus minimizing the power error.

5. Results

5.1. Test network

The proposed methodology is evaluated using the simulation model of the Sundom Smart Grid, a medium voltage distribution network located in Vaasa, Finland. Fig. 8 outlines the single line diagram of the Sundom Smart Grid. The primary substation connects the 110 kV and the 21 kV grids while the secondary substations connect 0.4 kV low voltage distribution networks to the power system. The grid encompasses approximately 2500 metering points, serving residential and small commercial consumers and comprises four feeders named J06 Sulva, J08 Wind, J09 Vaskiluoto and J07 Sundom [47]. The feeders contain both overhead lines (68.2 %) and underground cables (31.8 %) [48]. A 3.6 MW wind turbine is connected to the grid through a dedicated feeder J08 Wind. The details of the test network are presented in Table 5.

The Sundom Smart Grid served as a unique lab pilot, equipped with state-of-the-art intelligent electronic devices (IED). Collaborating closely with the University of Vaasa's Smart Grid laboratory, the Sundom grid facilitated direct communication and data collection, supporting a range of research activities. A cloud service was established to gather IEC 61850 sampled values and Generic Object-Oriented Substation Event (GOOSE) measurements from various points across the grid. In this research, the load profiles of the feeders and generation data from the wind turbine are extracted from these measurements as depicted in Fig. 9. Hourly average measured data over a period of one year, from May 1, 2017, to April 30, 2018, is used in this analysis.

5.2. Hosting capacity

To showcase the effectiveness of the proposed methodology,

Table 6
Simulation parameters.

Parameters	value
Population size	50
Maximum iterations	50
Photon rate	0.05
Range of v_{dbu}	1.05—1.09 pu
Upper limit of Q(U), $v_u{}^{max}$	1.15 pu
Range of slope (k_u)	4—48
Range of power factor	0.9–1
Installed DG capacity range, S_{DG}	2 MW – 16 MW
Voltage threshold, V^{max}	1.1 pu
Inverter oversizing, $S_{DG.os}{}^{max}$	11.12 %
Maximum wind generation	3.6 MW
Lumped minimum load on each feeder	J06 = 0.456 MW, J09 = 0.15 MW, J07 = 0.49 MW

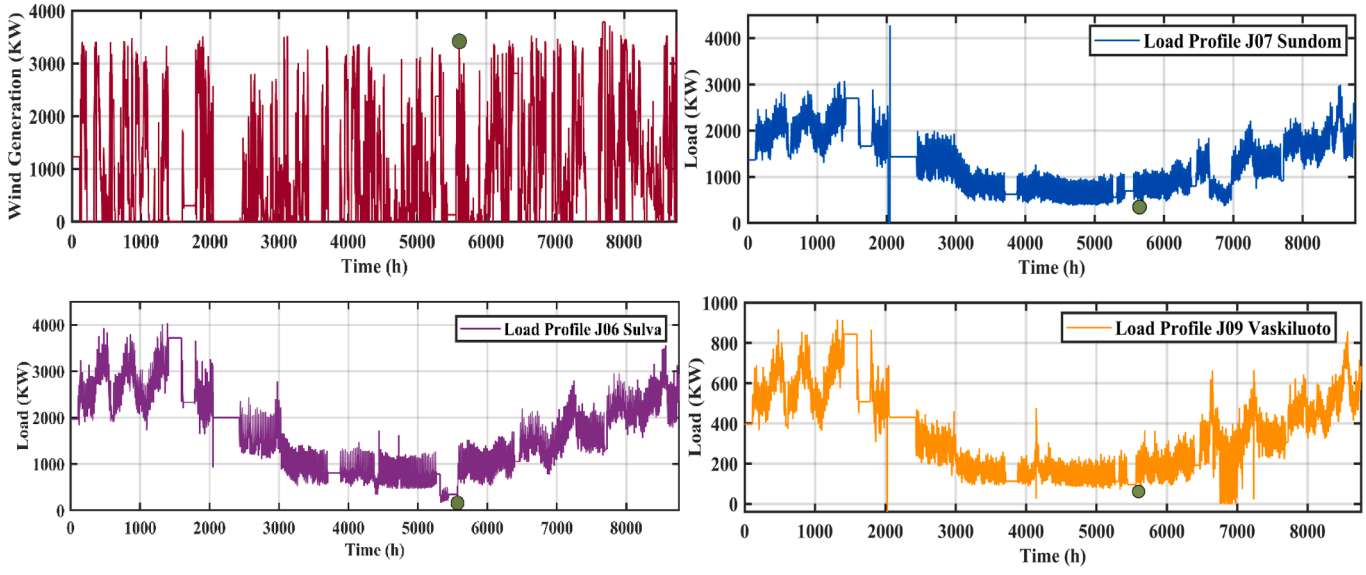

Fig. 9. Hourly measured Generation and Load data.

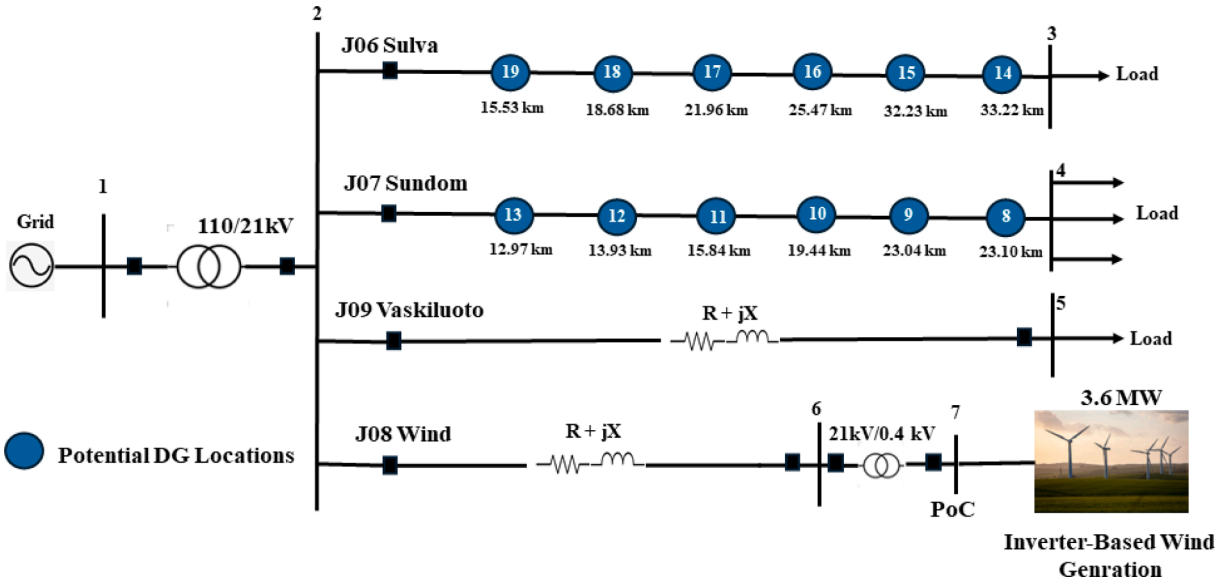

Fig. 10. Test network with potential DG locations.

Table 7
Detailed HC analysis of Sundom Grid.

Feeder J07 Sundom			Feeder J06 Sulva		
Location	Distance (km)	HC (MW)	Location	Distance (km)	HC (MW)
8	23.104	4.146	14	33.222	2.821
9	23.045	4.203	15	32.231	2.914
10	19.445	5.564	16	25.471	4.521
11	15.845	8.287	17	21.962	5.279
12	13.930	9.736	18	18.684	6.793
13	12.974	10.941	19	15.531	8.288

extensive simulations were conducted using MATLAB/Matpower software. The aim was to determine maximum DG capacity that can be installed in the Sundom grid without violating over-voltage and thermal loading limits of the feeder, while adhering to EN 50549 standards. The analysis was performed considering extreme operating conditions such as minimum load and maximum DG generation. The generation and lumped feeder load values used in this analysis are presented in Table 6 and marked with green circles in Fig. 9. Three test cases were executed to verify the effectiveness of the proposed method. In the case I, DGHC was examined considering DG size and location as decision variables without utilizing smart inverter control functions. In case II, smart inverter Cos Φ control mode was activated, and optimal location, size and power factor were determined to maximize the HC. In case III, smart inverter Q(U) control mode was activated and optimal volt-var control setpoints were determined to maximize the HC. In all cases the minimum installed capacity was set to 2 MW. Additionally, for a single DG the maximum installed capacity was capped at 16 MW, while for two DG units, it was constrained to 8000 kW. The simulation parameters are presented in Table 6.

Sundom grid contains 4 feeders: J06 Sulva, J08 Wind, J09 Vaskiluoto and J07 Sundom. Feeder J08 contains a wind turbine of 3.6 MW and in this analysis no more installation is considered on feeder J08. Feeder J09 is a small feeder of 7.035 km. The analysis on feeder J09 showed that HC was not limited by over-voltage curtailment and thermal loading constraints. Therefore, the proposed HC enhancement method was not applied on feeder J09. A comprehensive analysis on feeders J06 and J07 showed that overvoltage was the primary constraint limiting higher installed capacities. Furthermore, HC was significantly influenced by the location of the installed DGs. Therefore, six potential locations for DG installation were selected on each feeder (J06 and J07) based on

Table 8
Results for case I: No SI control.

Scenarios	Feeder J07 Sundom		Feeder J06 Sulva		HC (MW)
	Location/Generation (MW)		Location/Generation (MW)		
	DG # 1	DG # 2	DG # 1	DG # 2	
Scenario 1	13/10.94				10.94
Scenario 2	–	–	19/ 8.280	–	8.288
Scenario 3	13/10.793	–	19/ 7.990	–	18.783
Scenario 4	13/ 7.000	12/ 3.559	–	–	10.559
Scenario 5	–	–	19/ 5.223	18/ 2.101	7.324
Scenario 6	13/7.000	12/ 3.021	19/ 4.135	18/ 2.315	16.470

climatic, environmental, and topographical considerations as shown in Fig. 10. The HC analysis is presented in Table 7. The analysis results show that for feeder J07, the 13th location, situated nearest to the substation, enables the highest DG installation, whereas for feeder J06, 19th location permits the highest DG installation. The analysis clearly shows that HC tends to increase as the distance from the substation decreases.

The AOS algorithm was executed five times to generate results for the three test cases. The solution with the maximum HC value was selected as the optimal solution. For each test case, various scenarios were considered to evaluate the impact of single and multiple DG installations on the HC. In scenarios 1 and 4, feeder-level HC analysis was performed, considering one and two DG units on feeder J07, respectively. Similarly, scenarios 2 and 5 focused on feeder J06. In scenarios 3 and 6, grid-level HC analysis was performed by simultaneously installing DG units on both feeder J06 and feeder J07. Specifically, scenario 3 involved installation of one DG unit on each feeder, while scenario 6 involved two DGs on each feeder.

The results of case 1 are presented in Table 8, depicting scenarios with one and two DG units on each feeder. The results reveal that for feeders J07 and J06, the HC values of 10.941 MW and 8.288 MW are observed by installing DGs at 13th and 19th locations respectively. Furthermore, the highest HC value of 18.783 MW is achieved by installing one 10.793 MW DG on feeder J07 and another 7.99 MW DG on feeder J06. Notably, installing DGs on separate feeders yields higher HC values compared to deploying them on the same feeders. Moreover, when 2 DGS are installed on feeder J07, the hosting capacity value of 10.559 MW is achieved. Similarly, for feeder J06, a hosting capacity value of 7.324 MW is achieved by connecting two DGs at locations 19

Table 9
Results for case II: Cos Φ control.

Scenarios	Feeder J07 Sundom		Feeder J06 Sulva		HC (MW)
	Location/Generation (MW)/ {p.f}		Location/ Generation (MW)/ { p.f }		
	DG # 1	DG # 2	DG # 1	DG # 2	
Scenario 1	13/13.821/ {0.9}	–	–	–	13.821
Scenario 2	–	–	19/ 9.827/ {0.9}	–	9.827
Scenario 3	13/15.750/ {0.9}	–	19/11.608/ {0.913}	–	27.358
Scenario 4	12/7.314/ {0.913}	11/5.674/ {0.938}	–	–	12.988
Scenario 5	–	–	19/6.211/ {0.934}	18/2.347 / {0.951}	8.558
Scenario 6	12/6.936/ {0.913}	11/2.555/ {0.917}	19/7.081 / {0.964}	18/5.545 / {0.911}	22.117

and 18.

For Case II, the results shown in Table 9 underscore the effectiveness of Cos Φ control function in enhancing HC. In all considered scenarios, the smart inverter operates in inductive mode and absorbs reactive power. The results show that the highest HC value of 27.358 MW is achieved when one DG is connected at location 13 of feeder J07 and other DG is connected at location 19 of feeder J06. The optimally determined power factors are 0.9 and 0.913 respectively. The achieved HC is 45.65 % higher than the HC achieved in case 1. Furthermore, HC enhances to 12.988 MW when 2 DGs of 7.314 MW and 5.674 MW are connected at locations 12 and 11 of feeder J07 respectively. Similarly, installing 2 DGs at location 19 and 18 of feeder J06 results in HC increase to 8.558 MW, compared to 7.32 MW of case I.

The results for Case III, as outlined in Table 10, show the achieved hosting capacities values when Q(U) control is activated. When Q(U) control is activated, installing one and two generators on feeder seven yield hosting capacities of 13.817 MW and 12.987 MW respectively. The optimal location for a single generator scenario is 13, while for two generators, the optimal locations are 13 and 12. Similarly, for feeder six, the installed capacities for one and two generator scenarios are 9.826 MW and 8.558 MW respectively. The best outcome of 27.305 MW is attained when one generator of 15.730 MW is connected to feeder J07 and the other generator of 11.575 MW to feeder J06. Interestingly, in all cases, the maximum HC can be achieved by strategically placing a single DG unit on a distribution feeder, rather than connecting multiple DG units across two or three locations. Moreover, most of the determined optimal locations are found to be closer to the substation. The optimally determined Q(U) curves for various scenarios of Case III are depicted in Fig. 11.

For all considered cases, the convergence curves that represent maximization of objective function with the number of iterations are shown in Fig. 12. In the initial iterations, large fluctuations can be seen due to random initialization. However, these fluctuations gradually diminish when the exploration phase of the AOS algorithm concludes.

Table 10
Results for case III: Q(U) control.

Scenarios	Feeder J07		Feeder J06		HC (MW)
	Location/Generation (MW)/ { v_{dBu} , k_u}		Location/Generation (MW)/ { v_{dBu} , k_u}		
	DG # 1	DG # 2	DG # 1	DG # 2	
Scenario 1	13/ 13.817/ {1.077, 10.637}	–	–	–	13.817
Scenario 2	–	–	19/ 9.826/ {1.083,14.491}	–	9.826
Scenario 3	13/ 15.730/ {1.068, 6.246}	–	19/ 11.575/ {1.051, 5.105}	–	27.305
Scenario 4	13/ 7.290/ {1.050, 8.864}	12/ 5.699/ {1.050, 7.014}	–	–	12.987
Scenario 5	–	–	19 / 6.396/ {1.050,8.705}	18/ 2.155/ {1.062,9.132}	8.551
Scenario 6	13/ 6.119/ {1.081,5.043}	12/ 2.776/ {1.058,11.255}	19/ 6.750/ {1.077,13.081}	18/ 6.371/ {1.069,8.800}	22.016

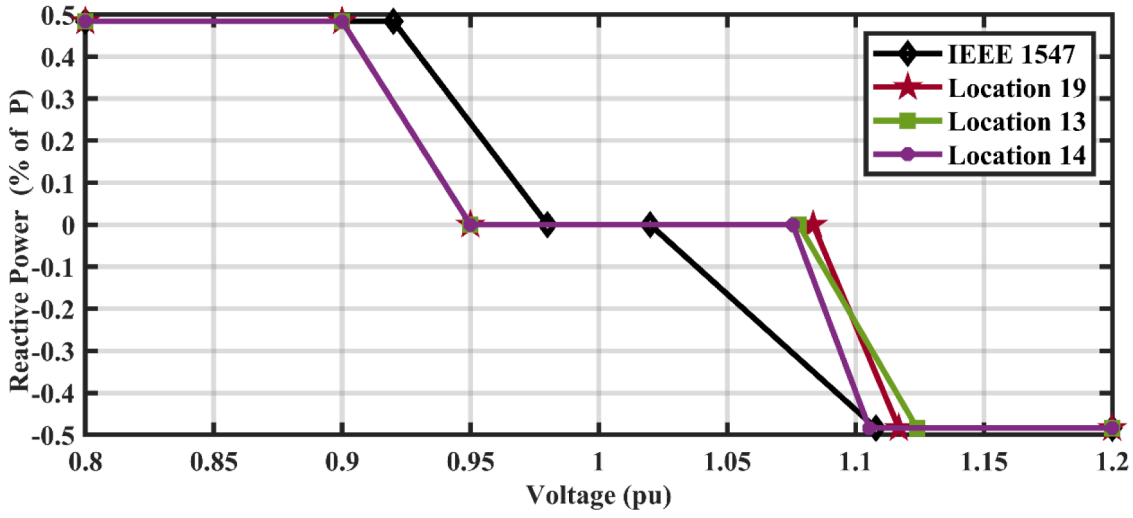

Fig. 11. Optimal volt/var settings determined by AOS optimizer at various locations.

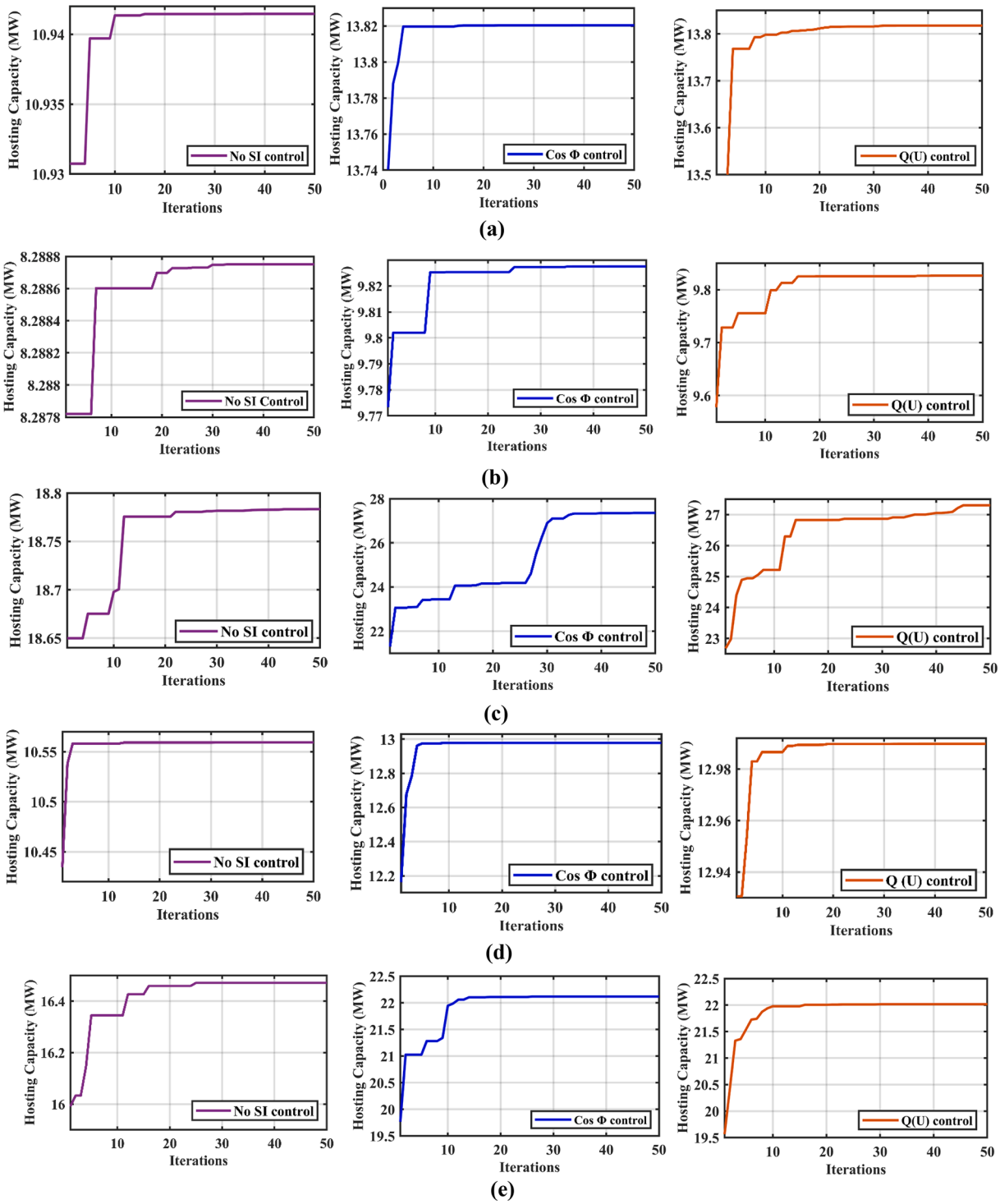

Fig. 12. Convergence curves for case I, case II and case III (a) Scenario 1 (b) Scenario 2 (c) Scenario 3 (d) Scenario 4 (e) Scenario 6.

Thereafter, the AOS algorithm swiftly converges towards global maxima leading to stable and consistent results. The results clearly show that the adaptive balance between global exploration and local exploitation ensures efficient exploration, rapid convergence, and optimal power extraction, ultimately enhancing overall hosting capacity.

To validate the effectiveness of the proposed AOS algorithm in HC computations, a comparative analysis was conducted against Slime mould algorithm (SMA) [49], Equilibrium optimizer (EO) [50], and Particle swarm algorithm (PSO) [51]. The convergence comparison plot for various algorithms is illustrated in Fig. 13. Fig. 13 (b) shows that the HC achieved by AOS is 27.35 MW, followed by SMA 27.18 MW, EO 27.13 MW and PSO 26.94 MW. Furthermore, each algorithm is independently subjected to twenty-five calculations, and the results of these computations are represented in the box plots, as depicted in Fig. 14. The results clearly show that AOS algorithm outperforms the comparative algorithms in terms of precision, stability, and reliability.

5.3. *DP-FCS-MPC based Q(U) and Cos Φ control.*

In this section, we delve into the implementation of Model Predictive

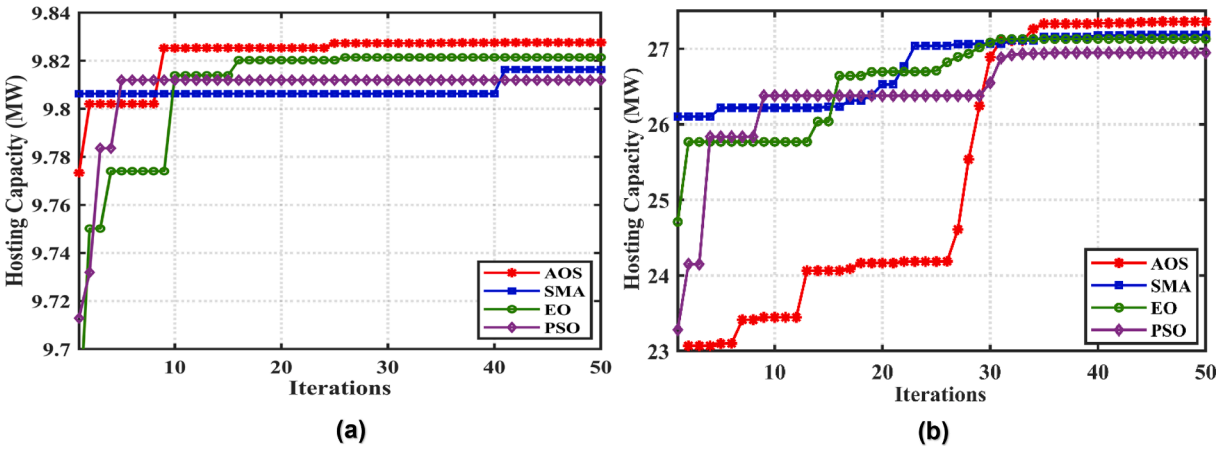

Fig. 13. Comparative analysis a) scenario 2b) scenario 3.

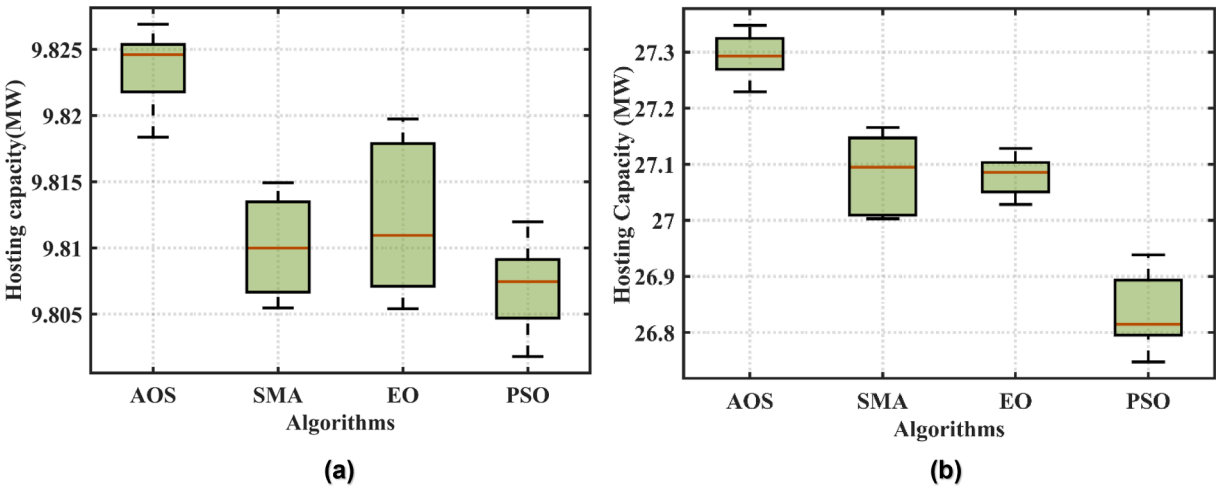

Fig. 14. Box Plot of various algorithms a) scenario 2b) scenario 3.

Table 11
Simulation parameters for DP-FCS-MPC controller.

Parameters	Value
Simulation platform	MATLAB Simulink
DC link voltage	1200 V
Sampling time	20 μsec
Inductance	2 mH
Resistance	0.084 Ω
Grid voltage	0.4 kV
Grid frequency	50 Hz

Control (MPC) aimed at augmenting hosting capacity. The aim was to design a Direct Power Finite Control Set Model Predictive Control (DP-FCS-MPC) system to regulate inverter switching in response to voltage violations. The real-world Sundom grid test network was replicated using MATLAB Simulink, considering the grid specifications elaborated in Table 6. The simulation parameters are shown in Table 11. To validate the efficacy of the proposed DP-FCS-MPC controller, a DG unit was installed at bus 3 of feeder J06 Sulva. The test network underwent simulations considering three operational modes: No smart inverter (SI) control, Q(U) control, and Cos Φ control. An optimizer block was integrated as a MATLAB function within the Simulink model. The optimizer block receives measurements from the Simulink model, estimates the system state, and computes optimal reference points for active power (P^{ref}) and reactive power (Q^{ref}). Subsequently, these reference points are dispatched to the DP-FCS-MPC controller. The DP-FCS-MPC adjusts inverter switching to track the reference signals sent by the optimizer whenever voltage violations arise. By dynamically optimizing the control actions of the DG unit, the MPC controller aims to alleviate voltage violations and amplify the hosting capacity of the grid.

A. Case 1: Optimal PQ management

This case evaluates the effectiveness of the proposed method for optimal *P* and *Q* management under specific load and generation conditions. The scenario was created by installing a DG at bus 3. Initially, the DG was generating 0.9 MVA of apparent power, and the voltage at the point of connection (PoC) was 1.033 pu. To analyze the response of the controller, the generation was increased to 2.9 MVA at t = 1.3 s. This additional generation caused the voltage at the PoC to rise to 1.103 pu, thereby violating the overvoltage limits as depicted in Fig. 15 (a). The voltages at the PoC, as well as the active and reactive power of the inverter system for Q(U) and Cos Φ control, are shown in Fig. 15 (b, c). It can be observed from Fig. 15 (b) that the Q(U) controller absorbs reactive power of 0.89 MVar at t = 1.3 s in response to the voltage rise, effectively reducing the voltage to 1.0986 pu, which falls within the acceptable limits. The optimal control setpoints are presented in Table 12. The optimal *P* and *Q* references were calculated by using Q(U) control setpoints in equation (3):

$$P^{ref} = S_{DG} = 2.9MW$$

$$Q^{ref} = S_{DG}{}^{*}\alpha\left(\left|v_{poc} - v_{dBu}\right|\right)k_u$$

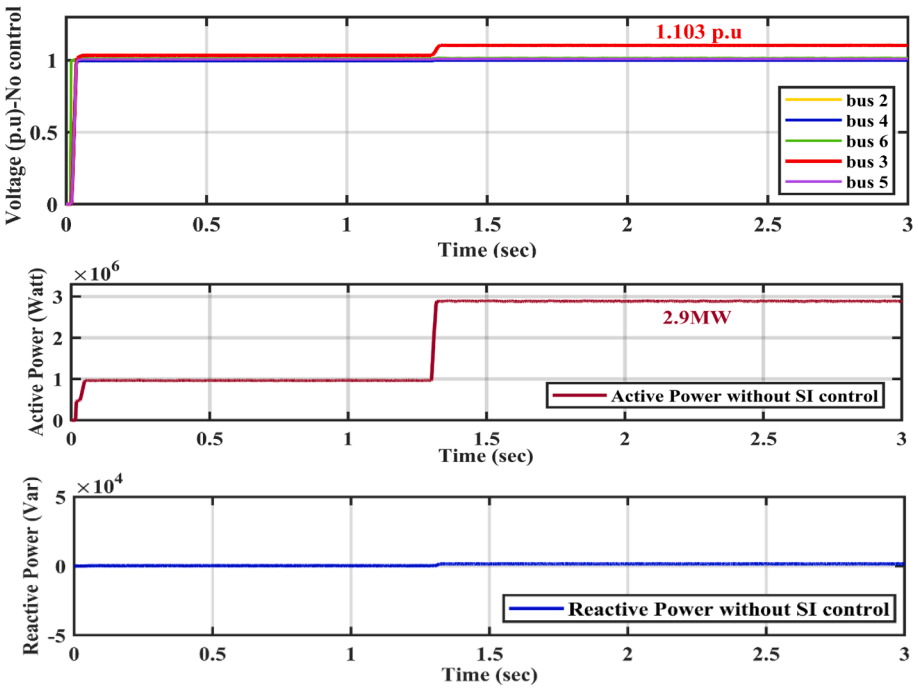

(a)

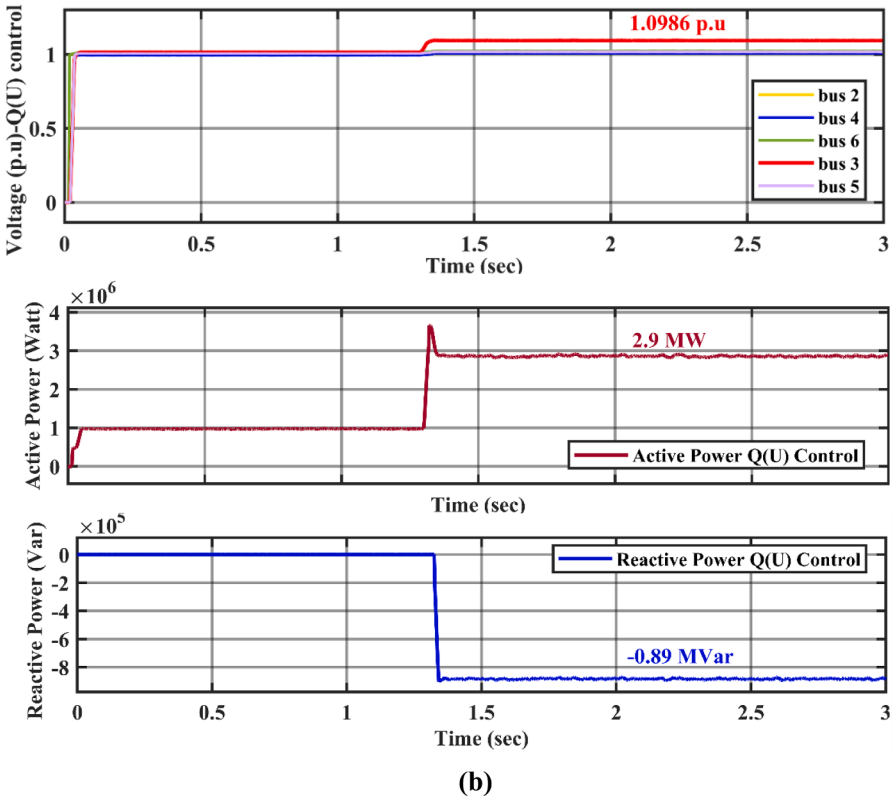

(b)

Fig. 15. Power and Voltage response for optimal PQ management (a) Considering No Smart Inverter control (b) Considering Q(U)control (c) Considering Cos Φ control.

$= 2.9*(-1)(1.1029 - 1.085)17.285$

$= -0.89MVar$

Similarly, Cos Φ control absorbed reactive power of 0.483MVar and curtailed active power to 2.859 MW in response to the voltage rise, resulting in a voltage reduction to 1.098 pu. The optimal P and Q references were determined by using Cos Φ control setpoints in equation (1):

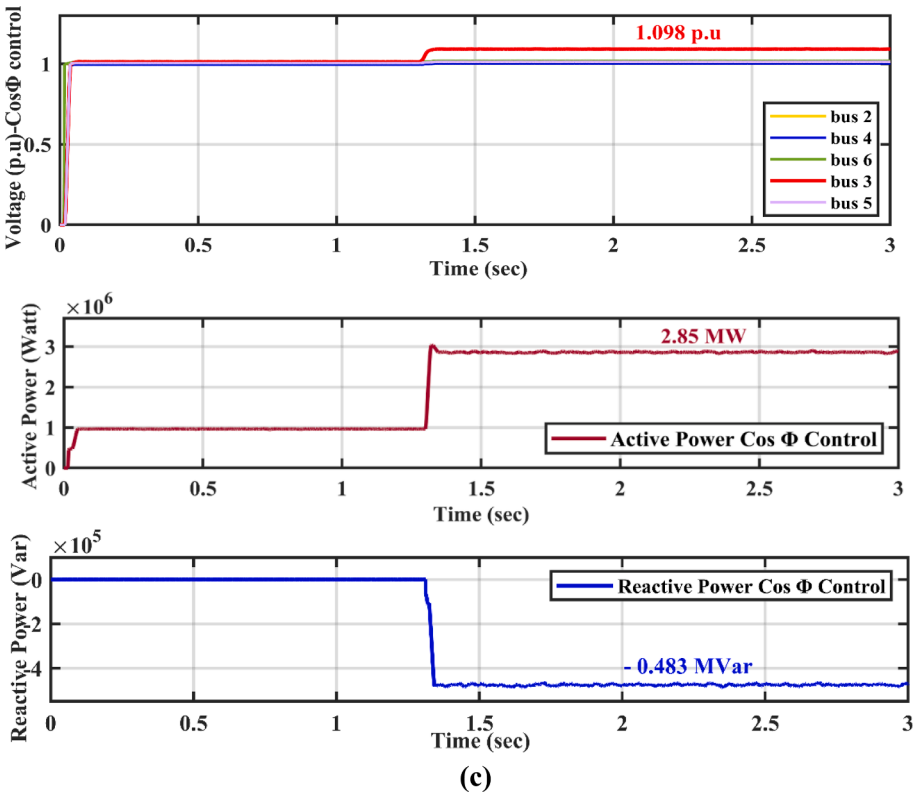

(c)

Fig. 15. (*continued*).

Table 12
Control setpoints for case 1 and case 2.

Case No.	Q(U) control	Cos Φ control
Case 1	$k_u = 17.28, v_{dBu} = 1.075$	$pf = 0.986$
Case 2	$k_u = 17.28, v_{dBu} = 1.075$	$pf = 0.90$

$$P^{ref} = S_{DG}{*}pf = 2.9{*}0.986 = 2.859MW$$

$$Q^{ref} = \alpha\left(P_{DG}{*}tan(cos^{-1}(pf)\right) = -1(2.859{*}0.169) = 0.483MVar$$

B. Case 2: HC capacity maximization

In this case, the effectiveness of DP-FCS-MPC based Q(U) and Cos Φ control for maximizing hosting capacity is validated. When smart inverter control functions were not considered, the maximum power that could be injected into the grid without violating the voltage limits was 2.8218 MW, as shown in Fig. 16 (a). However, with Cos Φ and Q(U) control, the inverter absorbed reactive power of 1.435 MVar and 1.434 MVar, respectively, to increase the hosting capacity to 2.966 MW and 2.963 MW, as shown in Fig. 16 (c) and 16 (b). These results clearly demonstrate that the proposed controller optimally selects inverter states to inject/absorb reference active and reactive power into the grid, thereby enhancing the hosting capacity.

Results of both considered cases show that DP-FCS-MPC strategy provides excellent transient and steady state response by efficiently tracking the reference active and reactive powers (P^{ref} & Q^{ref}) with minimum overshot. According to EN 50549 standards, the reactive power set value shall be reached within 10 s, with a maximum tracking tolerance of 5 %. The results clearly indicate that the proposed DP-FCS-MPC controller effectively maintains its tracking response within the specified bounds. Overall, results suggest that the proposed method has the potential to offer robust and efficient control in managing both active and reactive power in power systems.

Improving distribution network hosting capacity involves addressing several technical challenges, particularly with high penetration of DGS. Distributed generation causes voltage fluctuations and overvoltage issues, reducing the hosting capacity. MPC optimally adjusts reactive power (Q) from inverters to maintain voltages within limits. The proposed control framework proactively manages voltage levels, maximizes hosting capacity, and ensure grid stability under varying conditions. Traditional control methods often involve complex intermediate current loops, which can add to the system's design and operational complexity. This work emphasizes a decoupled power control mechanism without requiring intermediate current loops, simplifying the control architecture. Furthermore, by combining FCS-MPC with the AOS optimization, this work targets both precise power tracking and optimal distributed generation (DG) placement, enhancing network robustness.

6. Conclusions

This research comprehensively addresses the hosting capacity (HC) enhancement problem within the Sundom Smart Grid, spanning from the planning stage to controller-level implementation. Both feeder-level and grid-level HC analysis was performed considering extreme operating conditions such as minimum load and maximum generation. Results spotlight overvoltage as a primary constraint, particularly on feeders J06 Sulva and J07 Sundom, limiting higher installed capacities. Furthermore, HC was significantly influenced by the locations of the installed DGs. The maximum feeder-level HC was achieved by connecting single DG at the optimal location rather than installing multiple DGs at different locations on the same feeder. Moreover, grid-level hosting capacity analysis reveals that installing DGs on separate feeders yields higher HC values compared to deploying them on the same feeders. Also, HC tends to increase as the distance from the substation decreases.

The research also investigated smart inverter control modes, specifically Cos Φ and Q(U) control. The results show that HC increases by 45.65 % when SI control is activated. Notably, the effectiveness of SI

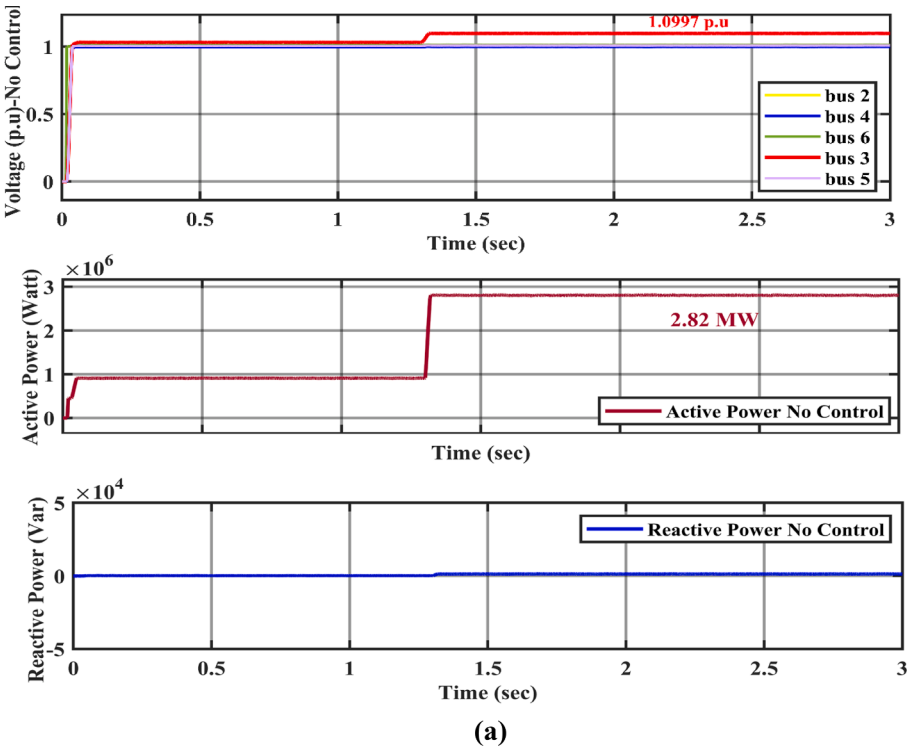

(a)

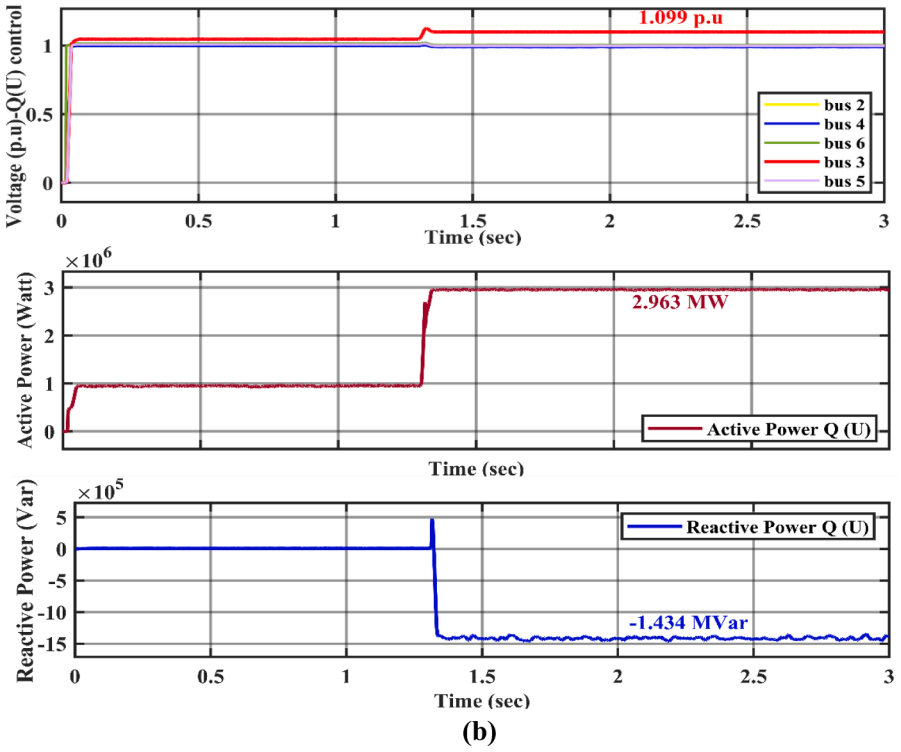

(b)

Fig. 16. Power and Voltage response for HC maximization (a) Considering No Smart Inverter control (b) Considering Q(U)control (c) Considering Cos Φ control.

control decreases as the distance from the substation increases, with Cos Φ mode exhibiting superior grid voltage support capabilities, albeit with some active power curtailment trade-offs. Additionally, the research proposes an optimal DP-FCS-MPC strategy for managing reactive and active powers, aimed at curtailing overvoltage and enhancing hosting capacity. Results indicate that the proposed optimal control framework provides a robust and efficient response within the bounds specified in EN 50549 standards. Given the absence of specific guidelines on smart inverter control setpoints in EN 50549, the proposed optimal control framework can be used by distribution system operators (DSOs) to make decisions regarding smart inverter control setpoints during voltage violations.

Author Statement

Muhammad Kamran Khan: Conceptualization, Methodology,

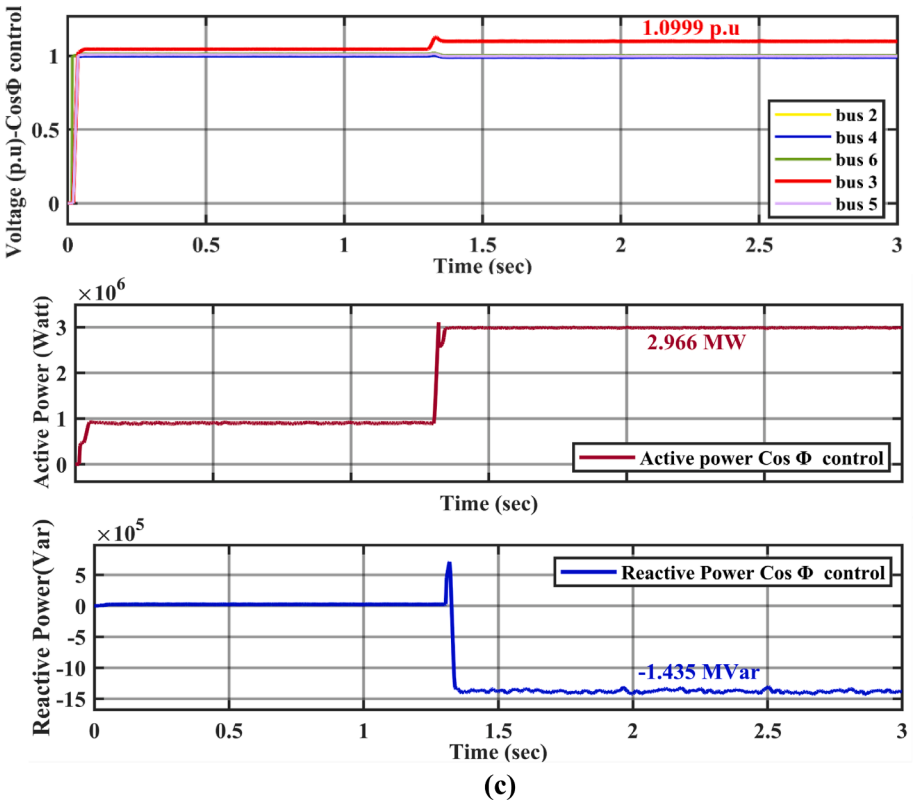

(c)

Fig. 16. (*continued*).

Writing- Original draft preparation, Software, Investigation. **Kimmo Kauhaniemi:** Visualization, Conceptualization, Writing – Review & Editing, Supervision, Validation, Resources. **Hussain Sarwar Khan:** Software, Conceptualization.

CRediT authorship contribution statement

Muhammad Kamran Khan: Writing – original draft, Methodology, Investigation, Data curation, Conceptualization. **Kimmo Kauhaniemi:** Writing – review & editing, Validation, Supervision, Resources, Project administration. **Hussain Sarwar Khan:** Software, Investigation.

Declaration of competing interest

The authors declare that they have no known competing financial interests or personal relationships that could have appeared to influence the work reported in this paper.

Data availability

Data will be made available on request.

References

[1] "Draft Paris Agreement." [Online]. Available: https://unfccc.int/files/bodies/awg/application/pdf/draft_paris_agreement_5dec15.pdf.
[2] Commission E. Summary of the Commission assessment of the draft National Energy and Climate Plan 2021–2030. Belgium: European Commission Brussels; 2020.
[3] Qamar N, Arshad A, Mahmoud K, Lehtonen M. Hosting capacity in distribution grids: A review of definitions, performance indices, determination methodologies, and enhancement techniques. *Energy Sci Eng* Apr. 2023;11(4):1536–59. https://doi.org/10.1002/ese3.1389.
[4] Mousa HHH, Mahmoud K, Lehtonen M. A Comprehensive Review on Recent Developments of Hosting Capacity Estimation and Optimization for Active Distribution Networks. *IEEE Access* 2024:1. https://doi.org/10.1109/ACCESS.2024.3359431.
[5] S. M. Ismael, S. H. E. Abdel Aleem, A. Y. Abdelaziz, and A. F. Zobaa, "State-of-the-art of hosting capacity in modern power systems with distributed generation," *Renew. Energy*, vol. 130, pp. 1002–1020, Jan. 2019, doi: 10.1016/j.renene.2018.07.008.
[6] "The interconnection bottleneck." [Online]. Available: https://www.cleanegroup.org/wp-content/uploads/Interconnection-Bottleneck.pdf.
[7] "Requirements for generating plants to be connected in parallel with distribution networks. Part 2: Connection to a MV distribution network. Generating plants up to and including Type B,SFS-EN 50549-2:2019.".
[8] "IEEE Standard for Interconnection and Interoperability of Distributed Energy Resources with Associated Electric Power Systems Interfaces.".
[9] "FINGRID,16.11.2018, Grid Code Specifications for Power Generating Facilities , VJV2018." [Online]. Available: https://www.fingrid.fi/en/grid/grid-connection-agreement-phases/grid-code-specifications/grid-code-specifications-for-power-generating-facilities2/.
[10] "IEEE 2030. 5 common California IOU rule 21 implementation guide for smart inverters,Common Smart Inverter Profile Version 1.0, 2016." [Online]. Available: https://sunspec.org/wp-content/uploads/2017/02/CSIPImplementationGuide-v1-0.pdf.
[11] Cho Y, Lee E, Baek K, Kim J. Stochastic Optimization-Based hosting capacity estimation with volatile net load deviation in distribution grids. *Appl Energy* Jul. 2023;341:121075. https://doi.org/10.1016/j.apenergy.2023.121075.
[12] Abideen MZU, Ellabban O, Ahmad F, Al-Fagih L. An Enhanced Approach for Solar PV Hosting Capacity Analysis in Distribution Networks. *IEEE Access* 2022;10:120563–77. https://doi.org/10.1109/ACCESS.2022.3221944.
[13] Trinh P-H, Chung I-Y. Integrated Active and Reactive Power Control Methods for Distributed Energy Resources in Distribution Systems for Enhancing Hosting Capacity. *Energies* Mar. 2024;17(7):1642. https://doi.org/10.3390/en17071642.
[14] Chathurangi D, Jayatunga U, Perera S, Agalgaonkar AP, Siyambalapitiya T. Comparative evaluation of solar PV hosting capacity enhancement using Volt-VAr and Volt-Watt control strategies. *Renew Energy* Nov. 2021;177:1063–75. https://doi.org/10.1016/j.renene.2021.06.037.
[15] Santos BLM, Barbosa D, Barros LS, Moreira FA. Photovoltaic Hosting Capacity Maximization of Low-Voltage Distribution Systems Based on Search of Optimal Power Factor for Interface Inverters Through Particle Swarm Optimization. *J Control Autom Electr Syst* Dec. 2023;34(6):1260–71. https://doi.org/10.1007/s40313-023-01043-z.
[16] Ding F, Mather B. On Distributed PV Hosting Capacity Estimation, Sensitivity Study, and Improvement. *IEEE Trans Sustain Energy* Jul. 2017;8(3):1010–20. https://doi.org/10.1109/TSTE.2016.2640239.
[17] Chang GW, Cong Chinh N. "Coyote Optimization Algorithm-Based Approach for Strategic Planning of Photovoltaic Distributed Generation," *IEEE. Access* 2020;8:36180–90. https://doi.org/10.1109/ACCESS.2020.2975107.
[18] Talkington S, Grijalva S, Reno MJ, Azzolini JA, Pinney D. A measurement-based approach to voltage-constrained hosting capacity analysis with controllable

reactive power behind-the-meter. *Electr Power Syst Res* Aug. 2023;221:109395. https://doi.org/10.1016/j.epsr.2023.109395.
[19] Jaramillo-Leon B, Zambrano-Asanza S, Franco JF, Soares J, Leite JB. Allocation and smart inverter setting of ground-mounted photovoltaic power plants for the maximization of hosting capacity in distribution networks. *Renew Energy* Mar. 2024;223:119968. https://doi.org/10.1016/j.renene.2024.119968.
[20] Chang GW, Chinh NC, Sinatra C. Equilibrium Optimizer-Based Approach of PV Generation Planning in a Distribution System for Maximizing Hosting Capacity. *IEEE Access* 2022;10:118108–22. https://doi.org/10.1109/ACCESS.2022.3220256.
[21] Purlu M, Turkay BE. Optimal Allocation of Renewable Distributed Generations Using Heuristic Methods to Minimize Annual Energy Losses and Voltage Deviation Index. *IEEE Access* 2022;10:21455–74. https://doi.org/10.1109/ACCESS.2022.3153042.
[22] Alturki M, Khodaei A, Paaso A, Bahramirad S. Optimization-based distribution grid hosting capacity calculations. *Appl Energy* Jun. 2018;219:350–60. https://doi.org/10.1016/j.apenergy.2017.10.127.
[23] Gush T, Kim C-H, Admasie S, Kim J-S, Song J-S. Optimal Smart Inverter Control for PV and BESS to Improve PV Hosting Capacity of Distribution Networks Using Slime Mould Algorithm. *IEEE Access* 2021;9:52164–76. https://doi.org/10.1109/ACCESS.2021.3070155.
[24] Shen K, Feng J, Zhang J. Finite control set model predictive control with feedback correction for power converters. *CES Trans Electr Mach Syst* Sep. 2018;2(3):312–9. https://doi.org/10.30941/CESTEMS.2018.00039.
[25] Lekouaghet B, Boukabou A, Lourci N, Bedrine K. Control of PV grid connected systems using MPC technique and different inverter configuration models. *Electr Power Syst Res* Jan. 2018;154:287–98. https://doi.org/10.1016/j.epsr.2017.08.027.
[26] Li X, Zhang H, Shadmand MB, Balog RS. Model Predictive Control of a Voltage-Source Inverter With Seamless Transition Between Islanded and Grid-Connected Operations. *IEEE Trans Ind Electron* Oct. 2017;64(10):7906–18. https://doi.org/10.1109/TIE.2017.2696459.
[27] Zhang Y, Jin J, Huang L. Model-Free Predictive Current Control of PMSM Drives Based on Extended State Observer Using Ultralocal Model. *IEEE Trans Ind Electron* Feb. 2021;68(2):993–1003. https://doi.org/10.1109/TIE.2020.2970660.
[28] Liu X, Qiu L, Rodríguez J, Wang K, Li Y, Fang Y. Learning-Based Resilient FCS-MPC for Power Converters Under Actuator FDI Attacks. *IEEE Trans Power Electron* Oct. 2024;39(10):12716–28. https://doi.org/10.1109/TPEL.2024.3416292.
[29] Bongard J, Berberich J, Köhler J, Allgöwer F. Robust Stability Analysis of a Simple Data-Driven Model Predictive Control Approach. *IEEE Trans Autom Control* May 2023;68(5):2625–37. https://doi.org/10.1109/TAC.2022.3163110.
[30] Liu X, Qiu L, Fang Y, Rodríguez J. Predictor-Based Data-Driven Model-Free Adaptive Predictive Control of Power Converters Using Machine Learning. *IEEE Trans Ind Electron* Aug. 2023;70(8):7591–603. https://doi.org/10.1109/TIE.2022.3208594.
[31] Liu X, Qiu L, Fang Y, Wang K, Li Y, Rodríguez J. Finite Control-Set Learning Predictive Control for Power Converters. *IEEE Trans Ind Electron* Jul. 2024;71(7):8190–6. https://doi.org/10.1109/TIE.2023.3303646.
[32] Liu X, Qiu L, Fang Y, Wang K, Li Y, Rodríguez J. Predictive Control of Voltage Source Inverter: An Online Reinforcement Learning Solution. *IEEE Trans Ind Electron* Jul. 2024;71(7):6591–600. https://doi.org/10.1109/TIE.2023.3303626.
[33] Nguyen HT, Kim E-K, Kim I-P, Choi HH, Jung J-W. Model Predictive Control with Modulated Optimal Vector for a Three-Phase Inverter with an LC Filter. *IEEE Trans Power Electron* Mar. 2018;33(3):2690–703. https://doi.org/10.1109/TPEL.2017.2694049.
[34] Merabet A, Labib L, Ghias AMYM. Robust Model Predictive Control for Photovoltaic Inverter System With Grid Fault Ride-Through Capability. *IEEE Trans Smart Grid* Nov. 2018;9(6):5699–709. https://doi.org/10.1109/TSG.2017.2694452.
[35] Bozorgi AM, Gholami-Khesht H, Farasat M, Mehraeen S, Monfared M. Model Predictive Direct Power Control of Three-Phase Grid-Connected Converters With Fuzzy-Based Duty Cycle Modulation. *IEEE Trans Ind Appl* Sep. 2018;54(5):4875–85. https://doi.org/10.1109/TIA.2018.2839660.
[36] Hu J, Zhu J, Dorrell DG. Model Predictive Control of Grid-Connected Inverters for PV Systems With Flexible Power Regulation and Switching Frequency Reduction. *IEEE Trans Ind Appl* Jan. 2015;51(1):587–94. https://doi.org/10.1109/TIA.2014.2328785.
[37] Yan S, Yang Y, Hui SY, Blaabjerg F. A Review on Direct Power Control of Pulsewidth Modulation Converters. *IEEE Trans Power Electron* Oct. 2021;36(10):11984–2007. https://doi.org/10.1109/TPEL.2021.3070548.
[38] Dutta A, Ganguly S, Kumar C. Coordinated control scheme for EV charging and volt/var devices scheduling to regulate voltages of active distribution networks. *Sustain Energy Grids Netw* Sep. 2022;31:100761. https://doi.org/10.1016/j.segan.2022.100761.
[39] Yang Y, Yeh H-G, Doan SH. Model Predictive Control via PV-Based VAR Scheme for Power Distribution Systems With Regular and Unexpected Abnormal Loads. *IEEE Syst J* Mar. 2020;14(1):689–98. https://doi.org/10.1109/JSYST.2018.2880362.
[40] Singh S, Pamshetti VB, Singh SP. Time Horizon-Based Model Predictive Volt/VAR Optimization for Smart Grid Enabled CVR in the Presence of Electric Vehicle Charging Loads. *IEEE Trans Ind Appl* Nov. 2019;55(6):5502–13. https://doi.org/10.1109/TIA.2019.2928490.
[41] Maharjan S, Khambadkone AM, Peng J-C-H. Robust Constrained Model Predictive Voltage Control in Active Distribution Networks. *IEEE Trans Sustain Energy* Jan. 2021;12(1):400–11. https://doi.org/10.1109/TSTE.2020.3001115.
[42] Li S, Sun Y, Ramezani M, Xiao Y. Artificial Neural Networks for Volt/VAR Control of DER Inverters at the Grid Edge. *IEEE Trans Smart Grid* Sep. 2019;10(5):5564–73. https://doi.org/10.1109/TSG.2018.2887080.
[43] I. Hamdan, A. Alfouly, and M. A. Ismeil, "Hosting capacity improvement for solar systems based on model predictive controller of volt-watt-var smart inverter functions," *Int. J. Model. Simul.*, pp. 1–15, Jul. 2023, doi: 10.1080/02286203.2023.2237400.
[44] Sousa JFB, Borges CLT, Mitra J. PV hosting capacity of LV distribution networks using smart inverters and storage systems: a practical margin. *IET Renew Power Gener* Jun. 2020;14(8):1332–9. https://doi.org/10.1049/iet-rpg.2019.1054.
[45] Zhang W, Sheng W, Liu K, Kang T, Zhan H. Toward optimal voltage/VAR control with smart PVs in active distribution networks. *Electr Power Syst Res* Mar. 2024;228:110076. https://doi.org/10.1016/j.epsr.2023.110076.
[46] Azizi M. Atomic orbital search: A novel metaheuristic algorithm. *Appl Math Model* May 2021;93:657–83. https://doi.org/10.1016/j.apm.2020.12.021.
[47] K. Sirvio *et al.*, "Controller Development for Reactive Power Flow Management Between DSO and TSO Networks," in *2019 IEEE PES Innovative Smart Grid Technologies Europe (ISGT-Europe)*, Bucharest, Romania: IEEE, Sep. 2019, pp. 1–5. doi: 10.1109/ISGTEurope.2019.8905578.
[48] K. Sirvio, L. Valkkila, H. Laaksonen, K. Kauhaniemi, and A. Rajala, "Prospects and Costs for Reactive Power Control in Sundom Smart Grid," in *2018 IEEE PES Innovative Smart Grid Technologies Conference Europe (ISGT-Europe)*, Sarajevo, Bosnia and Herzegovina: IEEE, Oct. 2018, pp. 1–6. doi: 10.1109/ISGTEurope.2018.8571695.
[49] Li S, Chen H, Wang M, Heidari AA, Mirjalili S. Slime mould algorithm: A new method for stochastic optimization. *Future Gener Comput Syst* Oct. 2020;111:300–23. https://doi.org/10.1016/j.future.2020.03.055.
[50] A. Faramarzi, M. Heidarinejad, B. Stephens, and S. Mirjalili, "Equilibrium optimizer: A novel optimization algorithm," *Knowl.-Based Syst.*, vol. 191, p. 105190, Mar. 2020, doi: 10.1016/j.knosys.2019.105190.
[51] Kennedy J, Eberhart R. "Particle swarm optimization," in *Proceedings of ICNN'95 - International Conference on Neural Networks*. Perth, WA, Australia: IEEE; 1995. p. 1942–8.